



TWO DIMENSIONAL POSITIONING AND HEADING SOLUTION
FOR FLYING VEHICLES USING A LINE-SCANNING LASER RADAR (LADAR)

THESIS

Brady Christel

AFIT/GE/ENG/11-04

DEPARTMENT OF THE AIR FORCE
AIR UNIVERSITY

AIR FORCE INSTITUTE OF TECHNOLOGY
Wright-Patterson Air Force Base, Ohio

APPROVED FOR PUBLIC RELEASE; DISTRIBUTION UNLIMITED.

The views expressed in this thesis are those of the author and do not reflect the official policy or position of the United States Air Force, Department of Defense, or the United States Government. This material is declared a work of the U.S. Government and is not subject to copyright protection in the United States.

TWO DIMENSIONAL POSITIONING AND HEADING SOLUTION
FOR FLYING VEHICLES USING A LINE-SCANNING LASER RADAR
(LADAR)

THESIS

Presented to the Faculty
Department of Electrical and Computer Engineering
Graduate School of Engineering and Management
Air Force Institute of Technology
Air University
Air Education and Training Command
In Partial Fulfillment of the Requirements for the
Degree of Master of Science in Electrical Engineering

Brady Christel, B.S.E.E.

March 2011

APPROVED FOR PUBLIC RELEASE; DISTRIBUTION UNLIMITED.

TWO DIMENSIONAL POSITIONING AND HEADING SOLUTION
FOR FLYING VEHICLES USING A LINE-SCANNING LASER RADAR
(LADAR)

Brady Christel, B.S.E.E.

Approved:

Michael Stepaniak

Lt Col Michael Stepaniak, PhD
(Chairman)

10 Mar 2011

date

M. Pachter

Dr. Meir Pachter (Member)

10 March, 2011

date

Gilbert Peterson

Dr. Gilbert Peterson (Member)

10 MAR 2011

date

Abstract

Emerging technology in small autonomous flying vehicles requires the systems to have a precise navigation solution in order to perform tasks. Where available, the Global Positioning System (GPS) is an excellent solution providing sub-meter level accuracy and drift free position using a small size receiver and low power consumption. In many critical environments, such as indoors, GPS is unavailable necessitating the development of supplemental aiding sensors to determine precise position. Small scale inertial measurement units are a popular solution, but suffer from significant error drift over time. To improve results, additional sensors are required.

This research investigates the use of a line-scanning laser radar (LADAR) as a standalone two dimensional position and heading navigation solution and sets up the device for augmentation into existing navigation systems. A fast histogram correlation method is developed to operate in real-time on board the vehicle providing position and heading updates at a rate of 10 Hz. A non-linear quadrotor simulator generates realistic flight profiles which are then used to produce LADAR scans as measured by a sensor on the vehicle. These simulations are then compared to experimental results collected using a SICK LD-OEM 1000.

The histogram correlation algorithm applied in this work was shown to successfully navigate a realistic environment providing a position accurate to 40 cm after 1 minute though additional aiding will be required to support long duration flights.

Acknowledgements

First, I would like to thank my advisor for suggesting the topic of this work, but more importantly the excellent guidance and insight provided throughout all steps of the process. I also thank my classmates for the constant bombardment of questions they endured and for their valuable input whenever I needed assistance. Finally, a special thanks to my family for their unending support throughout my entire education.

Brady Christel

Table of Contents

	Page
Abstract	iv
Acknowledgements	v
List of Figures	viii
List of Tables	xi
List of Abbreviations	xii
I. Introduction	1
II. Background	3
2.1 Motivation for MAV Flight	3
2.2 MAV Navigation Systems	3
2.3 Aiding Sensors	3
2.4 Self Localization	6
2.4.1 Reference Frames	6
2.4.2 Line and Feature Extraction	7
2.4.3 SLAM	8
2.4.4 Frame to Frame Correlation	8
2.4.5 Histogram Correlation	8
2.5 Aiding Navigation with Sensors	10
2.5.1 Kalman Filters	10
III. The Histogram Correlation Method	11
3.1 Scanner Data	11
3.2 Simulation	13
3.2.1 Background Setup	13
3.2.2 Scan Calculation	14
3.2.3 True Scanner Data Comparison	15
3.2.4 Reference Frames	17
3.2.5 Simulation in 3D	19
3.2.6 Quadrotor Simulator	20
3.2.7 Generation of Scans from Flight Profile	21
3.3 Histogram Method Calculation	22
3.3.1 Extraction of Vehicle Movement	27
3.3.2 Flight Attitude Effect On Range Measurement	28
3.3.3 Application of a Smoothing Filter	29
3.4 Line Extraction	30

	Page
IV. Performance Analysis	34
4.1 Simulation Results	34
4.1.1 Flight Profiles Used in the Simulation	34
4.1.2 Simulated Noise Levels	35
4.1.3 Update Rate Analysis	35
4.1.4 Smoothing Filter Selection	41
4.1.5 Comparison of 2 and 3 Dimensional Simulation	42
4.1.6 Extended Length Simulation Testing	46
4.2 Experimental Results	49
4.2.1 Device Setup	49
4.2.2 Realtime Data Display	50
4.2.3 Experimentation using Line Extraction	51
4.2.4 Data Collection	52
4.2.5 ANT Center Data Collection and Results	54
4.2.6 Hallway Data Collection and Results	58
4.3 Comparison of Simulated and Experimental Data	61
V. Conclusions and Recommendations	65
5.1 Conclusion of Performance	65
5.1.1 Simulation	65
5.1.2 Real World	65
5.2 Suggested Improvements to the Current Algorithm	66
5.2.1 Additional Filtering of Laser Scan Data	66
5.2.2 Integration with Additional Hardware or Software	67
5.2.3 Testing in a 3D Environment	67
5.2.4 Future Topics of Interest	68
Bibliography	69

List of Figures

Figure	Page
3.1. Simple Setup of an Experimental Room in Simulation	13
3.2. Simulated Laser Range Measurement	15
3.3. Full Laser Scan Measurement	16
3.4. ANT Center Simulation Layout	16
3.5. Statistical Analysis of Laser Scan Accuracies	18
3.6. Reference Frames Necessary to Operate LADAR on a Vehicle in a Navigation Frame	19
3.7. Quadrotor Body Frame and Attitude Angles	21
3.8. Angle Calculation Used in Histogram Algorithm	24
3.9. Histogram Correlation Method Matching Two Scans Taken in the ANT Center	26
3.10. Quadrotor Operation uses Small Pitch and Roll Angles Allowing the Application of the Small Angle Approximation	27
3.11. Scanner Measurements are Greater than or Equal to the True Distance to the Wall	29
3.12. Laser Scan Produced when Operation a Laser Scanner Near a Wall	30
3.13. Filtering the Scanner Data Provides both Good and Bad Effects	31
3.14. Hough Space representation: ρ, θ	32
3.15. Extracted Lines of from an LD-OEM 1000 Range Scan of the ANT Center	33
4.1. Profile 1 Simulation	37
4.2. Top Down View of Simulation Profiles Inside the ANT Center.	38
4.3. Comparison of Update Rates for Profile 1, Noise of 2 cm, and Filter Setting of 10	38
4.4. Comparison of Update Rates for Profile 3, Noise of 2 cm, and Filter Setting of 10	39

Figure		Page
4.5.	Monte Carlo simulations showing poor performance at an update rate at 1 Hz	40
4.6.	Filter Selection	41
4.7.	Mean Error in X and Y Direction	43
4.8.	Standard Deviation of Error in X and Y Direction	44
4.9.	Heading Mean Error and Standard Deviation	45
4.10.	Filter Setting	46
4.11.	2 D and 3 D Comparison of Simulation Profile 4	47
4.12.	2 D and 3 D Comparison of Simulation Profile 1	47
4.13.	Error Growth of A Longer Simulation Profile	48
4.14.	Beginning Time Stamps of LADAR Measured Data show Dropped Frames	50
4.15.	Two Consecutive Laser Scans in the ANT Center with Extracted Lines	53
4.16.	Experiment Setup with LD-OEM 1000 Laser Scanner Mounted on Cart with Trimble S6 Surveying System in the Foreground .	54
4.17.	Panorama of the ANT Center Showing 180 Field of View . . .	55
4.18.	Identical Scan of the ANT Center, as measured and filtered at a setting of 15	55
4.19.	Comparison of Trimble Observed and Histogram Correlation Estimated Trajectory	56
4.20.	Error Growth in Each Direction	57
4.21.	Estimated and Reference in X Direction Over Time	57
4.22.	Estimated and Reference in Y Direction Over Time	58
4.23.	Example of Angle Correlation while Traveling Down a Hallway	59
4.24.	Example of the Bad Direction for Translation Correlation as a Result of Traveling Down a Hallway	59
4.25.	Example of the Good Direction for Translation Correlation as a Result of Traveling Down a Hallway	60
4.26.	Estimated Path around Hallway using Different Filter Settings	60

Figure	Page
4.27. Poor Performance of the Algorithm While Traveling Down a Hallway	61
4.28. Simulated and Experimental Trajectory as Traveled in the ANT Center	62
4.29. Comparison using 2 cm noise estimate	63
4.30. Comparison using 4 cm noise estimate	63
4.31. Periodic Line Fit Error Caused by Interpolation of Trimble Data	64

List of Tables

Table	Page
2.1. LD-OEM 1000 Universal Laser Distance Scanner Technical Data	7

List of Abbreviations

Abbreviation		Page
UAV	Unmanned Aerial Vehicle	1
INS	Inertial Navigation System	1
MAV	Micro Air Vehicle	1
MEMS	Microelectromechanical System	1
GPS	Global Positioning System	1
LADAR	Laser Radar	1
LiDAR	Light Detection and Ranging	2
SLAM	Simultaneous Localization and Mapping	2
ANT	Advanced Navigation Technology	6
SIFT	Scale-Invariant Feature Transform	7
AFIT	Air Force Institute of Technology	15
DCM	Direction Cosine Matrix	17
ENU	East North Up	17
NED	North East Down	17
WGS84	World Geodetic System 84	19
ECEF	Earth Centered, Earth Fixed	19

TWO DIMENSIONAL POSITIONING AND HEADING SOLUTION
FOR FLYING VEHICLES USING A LINE-SCANNING LASER RADAR
(LADAR)

I. Introduction

Recent technology has pushed the development of unmanned aerial vehicles (UAV) to perform increasingly complicated tasks. These tasks require accurate knowledge of the vehicle's position and attitude. Larger aircraft are capable of carrying complex, albeit expensive inertial navigation systems (INS) with ring laser gyros and accelerometers able to maintain position to one or two miles even after several hours of operation [39]. However the navigation systems of micro air vehicles (MAV), a class of small UAV, do not have the resources to carry such systems and instead must use other methods for position information. A popular selection is microelectromechanical system (MEMS) devices because they are lightweight, compact, and generally low cost. These are subject to much larger error drift rates than other conventional systems. The global positioning system (GPS) provides meter-level accuracy and can significantly reduce the error drift of an onboard INS [29]. Unfortunately GPS is not always available in critical environments due to the restrictions of the system. Satellite reception necessary to calculate a position is not available indoors, underground, underwater, or even in harsh terrain such as dense forests and canyons. To overcome these issues and to attempt to limit the error growth, additional sensors are placed on MAVs to provide aiding information to the onboard navigation system. Sensors may also be added when GPS is available as they are able to observe higher frequency dynamics where GPS captures low frequency dynamics. Together they are able to provide a better navigation solution.

This thesis investigates the characteristics and limitations of an onboard line-scanning radar (LADAR) when operating in a 3 dimensional environment. This tech-

nology is also referred to as Light Detection and Ranging (LiDAR). These devices measure a range to an object often using infrared laser which is emitted, reflects off an object, and is then detected by the unit. Line-scanning LADAR measure numerous points around a circular field of view, often using a motor to spin a mirror to reflect the laser. Currently these are primarily used for navigation using Simultaneous Localization and Mapping (SLAM) techniques. These algorithms often require extensive processing power and data is post processed.

To avoid these limitations, a LADAR unit uses scan matching techniques to investigate an independent 2 dimensional position and heading solution suitable for use on a flying vehicle. To evaluate the potential of this system, several assumptions of the operation environment are made and the capabilities expanded as appropriate. Initially, the simulated environment is an indoor man made structure where there are parallel and perpendicular walls without obstructive objects. These results are then compared to experimental data collected in a realistic and cluttered environment.

The remainder of the thesis is organized as follows: Chapter 2 covers background information on the navigation and control systems of small flying vehicles along with previous research work performed. Chapter 3 details the complete problem solving approach including simulations used to evaluate LADAR as an aiding sensor. Chapter 4 provides results and quantitative analysis of the simulation. Chapter 5 draws conclusions and recommends future research.

II. Background

This chapter presents background information about micro air vehicle operation, the motivations for MAV flight, the navigation and control systems utilized by these, specifically the limitations of these systems derived from the vehicle, and various localization and mapping techniques used.

2.1 *Motivation for MAV Flight*

Micro air vehicles provide new opportunities and applications to unmanned vehicle operation. Examples for the motivations of civilian operation of these vehicles include remote search and rescue in hazardous areas, observation of difficult to observe construction sites such as bridges, or mobile weather observation platforms [16]. MAVs could also enable military applications such as autonomous surveillance or perform tasks in hostile areas.

2.2 *MAV Navigation Systems*

Large aircraft, such as airliners or military jets, are capable of carrying incredibly accurate self-contained yet expensive navigation system. Through the use of ring laser gyros and accelerometers the INS can determine it's position within 0.6 nautical miles after one hour or better [39]. However, these systems are not feasible on small air vehicles, not only because of cost, but also size and weight. Smaller versions of an INS often utilize MEMs devices which are nowhere near as accurate, and drift significantly [39]. For very short flights (less than a few minutes) they may be suitable, but problems arise quickly because of their large error bias and drift rates.

2.3 *Aiding Sensors*

The robotics community has been a driving force for localization and mapping techniques for many years. An investigation into a wide variety of sensors successfully implemented onto vehicles, along with the methods for navigation aiding, can be found in a University of Michigan report for the Oak Ridge National Lab D&D program [7].

While many of these techniques are optimized for land based vehicles, the technology can be adapted to flying vehicles. These vehicles also have the capability for the vehicle to act as a gimbal increasing a sensors potential without the addition of additional hardware such as a servo.

As previously mentioned, the nature of MAV flight restricts the type of equipment and sensors able to be flown. Issues include limited payload, electrical power, and processing capabilities available. Beyond these, operational environment also influences sensor selection. A desired sensor would not depend on the situation the vehicle is deployed, such as depending upon ambient light which is a problem with some vision based systems. It should also be non-destructive in any way. This includes physical contact with surrounding structures, or even radiation emitted from active sensors, such as vision damaging lasers. In military applications passive sensors are preferred because of they are not detectable to the enemy.

Accuracy of measurement systems is often a motivating factor in sensor selection. This is usually related to the wavelength of the signal used. Sonar or ultrasonic sensors, such as the LV-MaxSonar-EZ0, use 42 KHz signals to determine a range at a resolution of 1 inch [27]. LADAR systems generally use significantly higher frequencies in the infrared spectrum. A stationary non line-scanning device used for surveying can provide mm level accuracy with the appropriate processing [15].

Current rotating 3D LADAR systems are heavy and produce massive amounts of data, both a hindrance on MAV systems. A common example of this type of sensor, the Velodyne HDL-64E, uses 64 lasers to produce a 360 degree horizontal and 26.8 degree vertical field of view with an angular resolution of 0.09 degrees, and operates at a rate between 5 and 15 Hz. This results in over 1.3 million points per second which cannot currently be processed onboard an MAV. This device is incredibly popular in the DARPA Urban Challenge in which autonomous vehicles must navigate roads and obstacles [12,37]. A new version by Velodyne suits itself more for flying vehicles. The

HDL-32E LiDAR sensor measures 5.9 by 3.4 inches and weighs less than 3 pounds with production units shipping in the fall of 2010 [24].

Flash LADAR systems are a smaller alternative and produce a grid of depth measurements. For example, the Advanced Scientific Concepts TigerEye 3D flash LiDAR camera creates a 128 x 128 grid at a rate of 30 Hz with varying field of views and ranges. A 3 degree field of view yields up to 1100 m range measurements whereas a 45 degree field of view has a maximum range of 60 m [9]. A similar device, the Mesa Imaging SR-4000 was used to fit planes in an environment and assisted to constrain drift in an IMU [19].

Often, it is common to implement various sensors together to take advantage of their capabilities. For example a line-scanning LADAR and a camera are used to successfully navigate a cluttered room [4].

This thesis fully characterizes the line-scanning LADAR as a single sensor solution to determine a 2 dimensional position and heading. It expands on a current histogram correlation frame matching technique and investigates methods to optimize for operation in a 3 dimensional environment. This increases the flexibility when implemented on future systems.

A line-scanning radar was chosen because it fits within the limitations of a small flying vehicle and has extensive development in the ground based robotic vehicle field which is detailed later in this chapter. The most common unit used in many mobile robotics applications is the SICK Laser Measurement Sensor LMS-200 series. It is a 180 degree scanner with a range of 80 m. SICK has a few other models including a 360 degree variant, the LD-OEM 1000, which measures at a rate of 15 Hz and a range of over 100 meters. A higher speed scanner, the LMS-100, operates up to 50 Hz, but sacrifices range to 18 meters and is only able to measure up to a 270 degree field of view. Another company with competing scanning laser range finders is Hokuyo. The units used in robotics and flying vehicles are considerably smaller and lighter but suffer from reduced range and field of view. A commonly used scanner which was acquired

by the Advanced Navigation Technology (ANT) Center for another quadrotor, the URG-04LX, measures a 225 degree window inside the 270 degree available area at 10 Hz to a range of 4 meters but weighs only 5 ounces.

Similar work using line-scanning laser radar has shown promising results in the aiding performance of a 2D LADAR in a 3D environment [35]. Currently this work assumes a man made structure and performs plane fitting to the environment. This thesis provides the basis for a real time relative positioning method which avoids computationally restrictive SLAM elements which will be detailed in Section 2.4.3.

A specific sensor, the SICK LD-OEM 1000, was chosen for initial experimentation and simulation to analyze the technology currently available. The critical system specifications for this are shown in Table 2.1 [2]. Although this particular sensor is too large for most MAVs, the algorithms developed will apply equally to current and future devices which are smaller.

A common approach for extracting 3D data from a line-scanning radar is to use a servo to rotate the unit on its axis [6]. Other ideas include placing mirrors in front of the scanner to redirect the beam [30]. A similar method which does not use LADAR implements four single direction ultrasonic and two IR ranging sensors. It rotates in circles to generate a scan similar to a line-scanning LADAR and uses this data to proceed to the center of the room and map its shape [10].

2.4 Self Localization

Before detailing the specific techniques currently used with LADAR sensors, necessary background topics of robotic navigation and broad sensor data extraction methods will be discussed.

2.4.1 Reference Frames. Humans usually interpret navigation as to where an object, such as the quadrotor, is located in a room, or where they find their car traveling on a map. This is defined as the navigation frame. When a sensor on a vehicle makes a measurement it is unaware of its location in the navigation frame, and

Table 2.1: LD-OEM 1000 Universal Laser Distance Scanner Technical Data

Parameter	Value
Useful Scanning Angle	360°
Angular Resolution	0.125°
Scanning Frequency	5-15 Hz \pm 5% increments of 1 Hz
Measurement Resolution	3.9 mm
Beam Divergence Angle	2.5 mrad (0.143°)
Laser Diode	IR ($\lambda = 905$ nm)
Measurement Range (reflectivity of material)	
5% Relection (Black)	0.5 - 24 m
20% Reflection	0.5 - 50 m
90% Reflection	0.5 - 100 m
100% Reflectors	0.5 - 250 m

only has a reference to how it is mounted on the vehicle. This frame is designated the body frame. Additional reference frames are often necessary. The required reference frames used in this thesis, along with calculations and transformations are detailed in Chapter 3.

2.4.2 Line and Feature Extraction. Urban environments often provide structures with lines which are useful landmarks to be used for navigation. Early work included fitting line segments to environments using LADAR [38]. Numerous other methods have been developed and a few of the algorithms are compared by Nguyen et al [31]. These methods include an incremental method where points are added to a line until the next consecutive point no longer satisfies specified conditions. Others use a sliding window of points to fit line segments to points. Once all segments are generated colinear segments can be merged into lines.

Vision based systems have more information available due to a full frame of color information but can use similar techniques. Scale-Invariant Feature Transform (SIFT) is commonly used to detect features in an image. After processing using this algorithm high-contrast points in an image are determined and can be matched across multiple images to produce estimates of movement and attitude change. Similar algorithms such as the Canny edge detection method can be applied to detect lines.

2.4.3 SLAM. Simultaneous Localization and Mapping (SLAM) is a concept used by autonomous robots to attempt to build a map of an unknown environment as it navigates. The robot must have an accurate model of its system dynamics along with sensors to provide observability to features and landmarks in the area. These features, such as walls or stationary objects are detected by a sensor and placed into a map according to the robots current estimated position, often estimated using odometry. LADAR, vision based cameras, or sonar devices can be used to extract features. When a robot returns to a location previously mapped it is able to recognize identical features and adjust its position estimate bounding the growth in errors developed over time such as those caused by wheel slip, or measurement drift in an IMU.

2.4.4 Frame to Frame Correlation. Avoiding computation and memory storage elements required in SLAM, frame to frame correlation is used as an alternative method to processing vision or LADAR based measurements. Consecutive sensor measurements can be compared to determine movement or attitude change in real time due to reduced computational requirements. Disadvantages to this approach include unbounded error growth. Complex correlation methods using probabilistic approaches requiring intense computation were implemented in real-time using parallel processing of graphics processing units and outperformed many other correlation methods [32].

2.4.5 Histogram Correlation. An alternative to complex and computation hungry SLAM or probabilistic algorithms takes a different approach. The histogram method is a frame to frame correlation technique which uses two consecutive LADAR scans to find the rotation and translation of the vehicle [42]. This is explained in detail in Chapter 3. A brief synopsis follows:

The scanner data, provided in polar coordinates, is first mapped to the Cartesian body frame. Each set of consecutive points forms a line segment and its angle is calculated in relation to the scanner (body) frame. These angles are then collected into a histogram with bins of the calculated angle. When operating in man made

environments where one can assume near perpendicular and parallel walls this results in significant peaks in the histogram.

In the absence of translation and measurement noise, two scans will be identical except for a phase shift. Noise and movement will cause subtle differences but performing a correlation between the two scans will result in the rotation angle. There are known cases such as a large rotation which may fail correct detection with this method, but there are ways to mitigate this. One method is to limit the search window based on an additional sensor's estimate (MEMs gyro), or using different algorithms [22].

Upon calculation of the vehicle's rotation between the consecutive frames two additional histograms are formed to determine translation in two orthogonal directions. First, the measurements of one scan are rotated by the calculated rotation angle so that the scans lie in the same orientation in the navigation frame. Then, an x-direction and y-direction histogram are used to determine a Δy and Δx translation. These correspond to movement of the vehicle in the body frame which can then be transformed to the navigation frame [42].

Advantages to the histogram approach are avoiding costly line or feature detection algorithms while mitigating the effects of sensor noise. Also, moving objects in the measurement area do not degrade performance significantly. This method was shown to assist in the construction of accurate maps in real time, using a Pentium III-600 computer [34].

One proposed improvement to the algorithm, especially in cases where there is a large rotation between frames, uses vector histogram matching [22]. Another modification successfully mapped an unknown outdoor environment [8]. Other developments of these algorithms claim to greatly improve calculation speed, with future work laid out to improve accuracy of scan matches [33].

This thesis investigates the use of a method originally designed to use onboard driving robotic vehicles. These vehicles have access to odometry information which

assists overall performance with an independent estimate of the vehicle's dynamics. A different LADAR than often used with this algorithm utilizes a higher resolution and 360 degree field of view to apply a similar algorithm to determinate a relative positioning solution. The additional observability and range measurements from the scanner improve the devices capability to produce a standalone position and heading solution. The research is then extended to consider the effects of small attitude changes as are typical of rotary aircraft.

2.5 Aiding Navigation with Sensors

2.5.1 Kalman Filters. The presence of noise and inaccuracies in all sensor measurements motivate the use of a Kalman filter in aircraft navigation systems. It produces optimal estimates of the vehicle states by using a three step process. First, the system states are estimated using a model, then the expected uncertainty in these estimates is calculated, and finally the incoming measurements are weighed appropriately before incorporating them into the state estimate. If implemented correctly, this process also helps capture some of the unknown errors associated with drifts and biases in the IMU [28].

III. The Histogram Correlation Method

This chapter outlines the process used to transform sensor data into a navigation solution. First, a simulation was developed in two dimensions to observe how the different algorithms used by mobile robots perform. After selection of an algorithm the simulation will be expanded into 3 dimensions where imitated flight trajectory and attitude information can be implemented. These allow the generation of realistic LADAR data scans identical to those produced on the vehicle. Different processing methods can then be applied to these laser scans and evaluated in performance of determining a position and heading.

3.1 Scanner Data

Line-scanning LADAR systems measure only a distance from the scanner to the first object in it's path using radio frequencies usually in the ultraviolet, visible, or infrared range. The two most common methods are using time of flight and phase based measurements. In a time of flight system the distance is calculated using Equation 3.1:

$$\text{distance} = \frac{\text{Speed of Light} \times \text{Time of Flight}}{2} \quad (3.1)$$

These sensors measure data up to 1500 m and are accurate to 1-10 cm. Phase based systems produce measurements accurate to a few mm but are limited to a range of 70 m [15].

To increase a ranging sensor's usefulness a motor is used to spin some element of the scanner, usually the mirror, allowing measurements to be collected up to a 360 degree field of view. Typical accuracy of the systems used on mobile robots, depending on the reflectivity of the object and the distance between the object and the scanner, is a few to ten centimeters with minimal angle uncertainty. In [5] these errors are detailed in great length regarding the SICK LMS-200. Similar analysis is

not available for the LD-OEM1000 but similar errors are expected to be present in most line-scanning LADAR devices.

Data generated by a LADAR unit is in polar coordinates consisting of an angle, θ , and a range, r . The angle is rarely transmitted by the scanner but relies on the user to account for this. A simple transformation is used to convert it into Cartesian coordinates is:

$$\begin{aligned}x &= r \sin(\theta) \\y &= r \cos(\theta)\end{aligned}\tag{3.2}$$

where x and y are the Cartesian coordinates, r is the measurement range, and θ is the angle.

The SICK LD-OEM 1000 unit has the capability to utilize a user defined scan area, resolution, and scan rate. These are restricted due to hardware capabilities and limited by the pulse frequency of the laser diode in the unit to avoid damage caused by heat. The maximum pulse frequency is limited to 14.4 kHz with a maximum mean pulse frequency over one scan of 10.8 kHz. For this application a constant measurement resolution across the whole 360 degree area of view will be used. A common setting for this type of application, and the one used for the majority of this work, is 1/2 degree resolution scanning a full 360 degree revolution at a rate of 10 Hz [1].

When using LADAR data during the operation of a vehicle, usually one complete revolution of the scanner is used as a single piece of data. This may be compared to another complete scan, or by using a SLAM based approach where each scan is linked to an environment map and features are tracked across the full scan history. To investigate the performance of LADAR operating in a dynamic flight environment a simulation using MATLAB® was developed. Performance in the simulation is then compared to data collected in a real environment.

3.2 Simulation

3.2.1 Background Setup.

Using a simulation for initial investigation of LADAR performance provides the opportunity to test various environments and sensor capabilities before unknown real world effects degrade performance. The first step was to develop a technique to represent an environment. In two dimensions a line segment is the simplest feature to implement by designating two coordinate points in the navigation frame. For simplicity, the first two walls of a 100 meter square room are shown in Figure 3.1. Another shape of interest is a circle. This may represent an obstruction in the room such as a support pole, or even a rough estimate for a person standing in the room. To represent this a coordinate point and a radius defines a circle. Besides the room structure to represent various environments, a scanner struc-

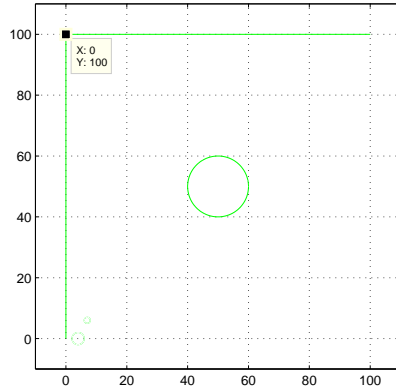


Figure 3.1: Simple Setup of an Experimental Room in Simulation. Two walls of a 100 meter square room. The coordinate pairs for the line segments are (0,0) to (0,100), and (0,100) to (100, 100). The circle in the center is at point (50,50) with a radius of 10.

ture was developed to easily change sensor characteristics such as range or noise on the measurements. The primary variables are the range ρ , measurement noise, σ_n , and resolution (angular step width). When movement of the scanner is implemented the scan frequency of the unit is also necessary.

One additional structure is required to represent the vehicle and measurement system in the body frame. To perform a scan the vehicle state must be defined with an x and y position (P_x , P_y), and the vehicle heading (ψ_v). Velocities and angular rates are necessary for moving vehicles. An alternative is to externally generate the flight profile and vehicle states over time and then import these into the simulation to generate scan data. If the LADAR is not placed at the center of the vehicle a vector addition must be performed to account for the offset. Likewise, if the scanner and body heading are not the same, the difference must be accounted for. These cases may introduce degraded performance as a rotation of a vehicle will cause an undesirable LADAR position trajectory when the scanner does not move in a straight line during the scan. For simplicity, the scanner position will be collocated with the origin of the body frame.

3.2.2 Scan Calculation. With the environment, scanner characteristics, and vehicle state defined, the LADAR is ready to perform a simulated scan. The sensor heading defines where the first measurement is taken (0 degrees in the body frame). The LD-OEM 1000 rotates counterclockwise, so its heading is opposite the vehicle, where a counterclockwise rotation is positive in magnitude. The laser measurement is modeled as a line segment from the vehicles current position, to the point at it's maximum detection range, at the current angle. This is detailed in Figure 3.2 and calculated as follows:

$$\begin{aligned}(x_1, y_1) &= (P_x, P_y) \\ (x_2, y_2) &= (P_x + \rho \cos(\psi_m), P_y + \rho \sin(\psi_m))\end{aligned}\tag{3.3}$$

where (x_1, y_1) is the vehicle position and (x_2, y_2) is the maximum measurement point of the scanner at its current orientation. ψ_v , the vehicle's heading, and ψ_s the scanner current angle, are added together to determine ψ_m , the measurement angle.

Next, this scanner line segment must be checked to see if a measurement occurs. It is checked for a collision against all elements of the environment structure. To

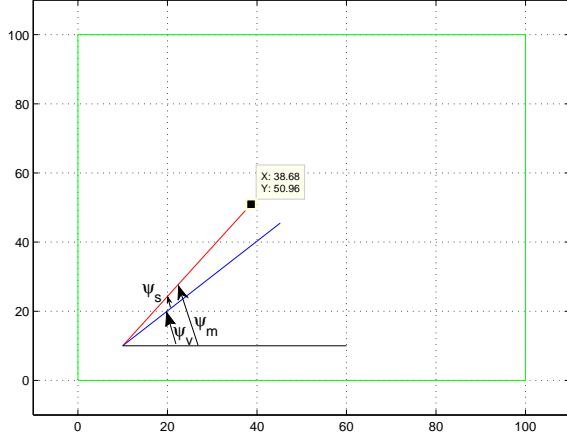


Figure 3.2: Simulated Laser Range Measurement. This figure represents a simulated measurement from a LADAR unit in the previously defined room at a position of (10,10). The vehicle heading of -45 degrees, ψ_v , is added to the scanner heading, ψ_s , of 10 degrees, and the measurement calculates a line segment in the navigation frame from the unit to its range of 50 meters.

perform the necessary calculations for two dimensional line to line, and line to circle intersections, Kevin Lindsey’s JavaScript code was ported to MATLAB [25]. If an intersection was found the simulation keeps track of the distance and coordinate point that this occurs. After checking all possible objects in the environment only the shortest distance is recorded. If there is a sensor noise attribute it is added at this point as a Gaussian random variable to the measurement range, and it’s coordinate pair is also recorded. This method of adding noise assumes perfect measurement angle alignment in the sensor. Figure 3.3 shows a simulated scan of the environment detailed above. This noise method for adding measurement noise was verified with real data, and is detailed in the next section.

3.2.3 True Scanner Data Comparison. To verify the simulated laser scan generation method the LD-OEM 1000 was setup to take measurements in the ANT Center at the Air Force Institute of Technology (AFIT). The walls of the ANT Center were measured and mapped to the nearest meter. The room is a horseshoe shape due to a temporary office setup with portable walls in the center. It also has long hallways

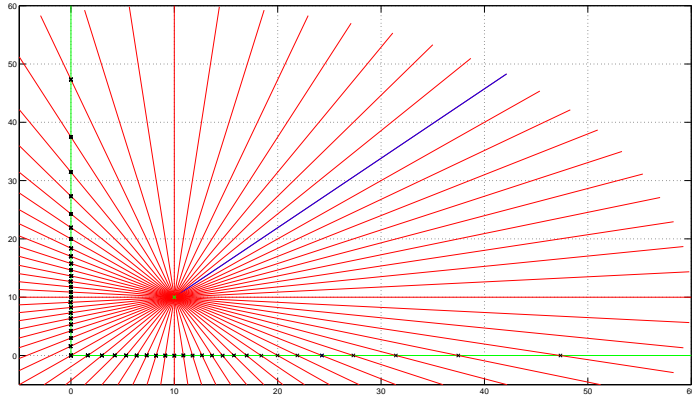


Figure 3.3: Full Laser Scan Measurement. This figure represents a laser scan of the vehicle at position (10,10) and every 5 degree measurement shown in red. A black x represents the measured point of the intersection with a Gaussian noise of 2 cm which is not noticeable at this scale.

just outside the entrance. To provide a simple model of these hallways they extend 100 meters in both directions and are included in the top-down simulation map as shown in Figure 3.4.

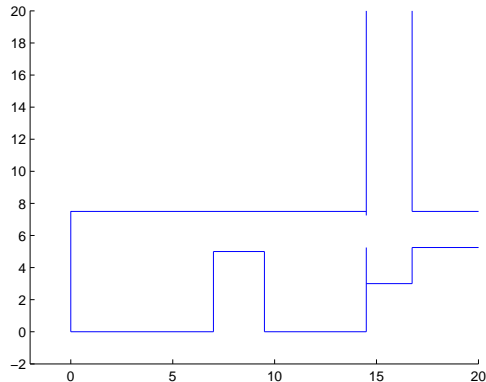
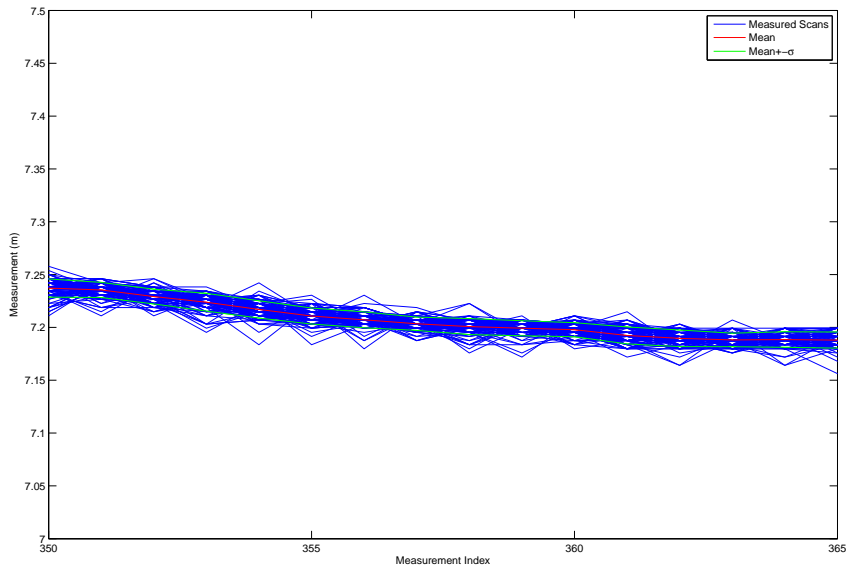


Figure 3.4: ANT Center Simulation Layout

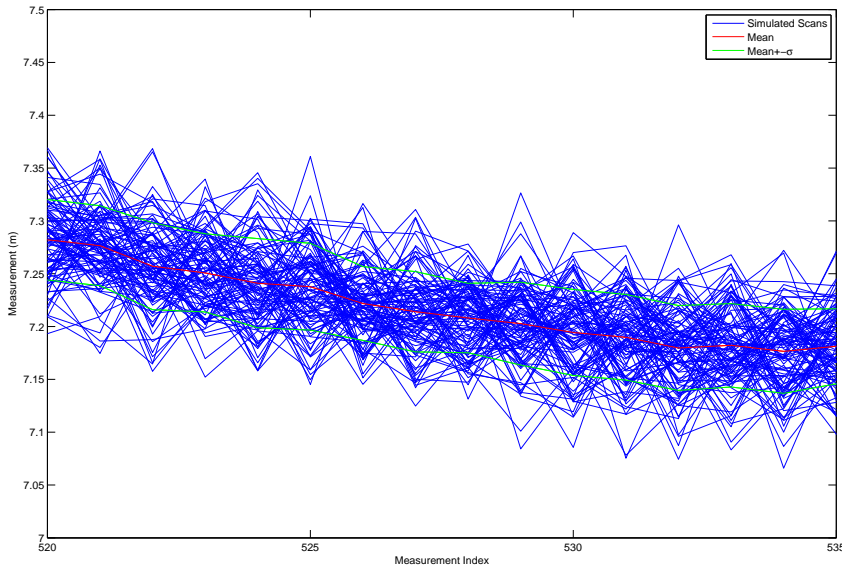
The LD-OEM 1000 online data sheet claims a $1-\sigma$ statistical error of ± 25 mm, a systematic error of ± 38 mm, and a resolution of 3.9 mm. This resolution, where the discrete measurements can occur, is visible in Figure 3.5(a). Since no truth measurements are available at this accuracy only the precision of the scanner can be analyzed using this method. The simulated scans, Figure 3.5(b), were performed with

an additive white Gaussian noise of strength 38 mm. The truth scan performed much better than expected compared to the errors quoted on the datasheet. The average calculated standard deviation over 100 scans, calculated for each measurement point, was 0.91 cm for the experimental data. For the simulated laser scans the noise was near expected at 3.77 cm. This indicates that the sensor may perform better than the original expectation of a noise of 3.8 cm. The accuracy is said to degrade with greater measurement distance from the scanner which can attributed to the systematic error [2].

3.2.4 Reference Frames. A human operating an air or land vehicle is likely to be interested in its position in the environment, or navigation reference frame, whether it be determining which street they are driving on, or if they are operating an aircraft in a restricted airspace. In these cases the operator is able to use visual cues, maps, or other devices to aid in the determination of the approximate location. An autonomous vehicle is unable to use these and must use sensors to approximate its position. Most sensors operate in the body reference frame and have minimal knowledge of the navigation frame. One example, a forward looking camera mounted on the nose of an aircraft has a limited observability of the nav frame at any time, but it does have a constant field of view in relation to the body frame. An exception to this is a GPS device which provides a position solution in the navigation frame, but at the same time offers limited information in the body frame such as aircraft attitude. In order to perform calculations across reference frames a Direction Cosine Matrix (DCM) is used. This is time dependent and changes with the vehicle's state. These calculations are further detailed in Section 3.2.7. The body frame of a flying vehicle is often defined by the x-axis going from the center of the body out the nose, the y-axis points through the right wing, and to complete a right handed coordinate system the z-axis points down. The navigation frame used in this thesis will consist of a common East, North, Up, or ENU, coordinate frame. Another option is the North, East, Down, or NED, frame. These axes are defined in a specific order, (x,y,z), to



(a) 100 Stationary Scans of LD-1000 Laser Rangefinder with Mean and Standard Deviation Shown



(b) 100 Simulated Stationary Scans at a Noise of 38 mm with Mean and Standard Deviation Shown

Figure 3.5: Statistical Analysis of Laser Scan Accuracies

be consistent with orthogonal right-hand coordinate frames. Vehicles which fly faster or further during the duration of the flight use another common reference frame, the

World Geodetic System 1984, (WGS84) which is in the class of reference systems called Earth Centered, Earth Fixed (ECEF) where the origin is the center of mass of the Earth, and a point is defined by a point on the Earth in latitude, longitude, and altitude. This is the frame that GPS provides a position solution [29]. Figure 3.6 shows the relation of the reference frames necessary for this thesis.

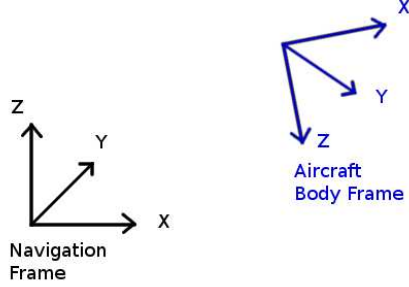


Figure 3.6: Reference Frames Necessary to Operate LADAR on a Vehicle in a Navigation Frame

In this thesis the measurement frame, the frame in which the LADAR takes measurements, is defined to be collocated with the body frame. Otherwise, transformation between the navigation and measurement frame would be accomplished using a DCM from the navigation to body frame followed by a DCM from the body to measurement frame, and vice versa for the opposite transformation.

3.2.5 Simulation in 3D. Upon confirming that the simulated laser scans suitably matched the scanner it was necessary to expand into a flying (3D) environment. First, the ANT Center needed to be expanded and represented in three dimensions. The existing layout was used for the walls and hallways. Instead of being represented as a line, each wall was defined as an infinite planar surface. To define its limits another matrix was stored into the environment structure accounting for the minimum and maximum x, y, and z values for each wall which is referenced when checking for a measurement intersection. With the new measurement consisting of

checking between a line segment and a plane a 3D geometry toolbox, geom3d, was implemented for simplicity and accuracy [23]. To complete the environment structure of the ANT center, a floor and ceiling were placed as a flat plane 3 meters apart.

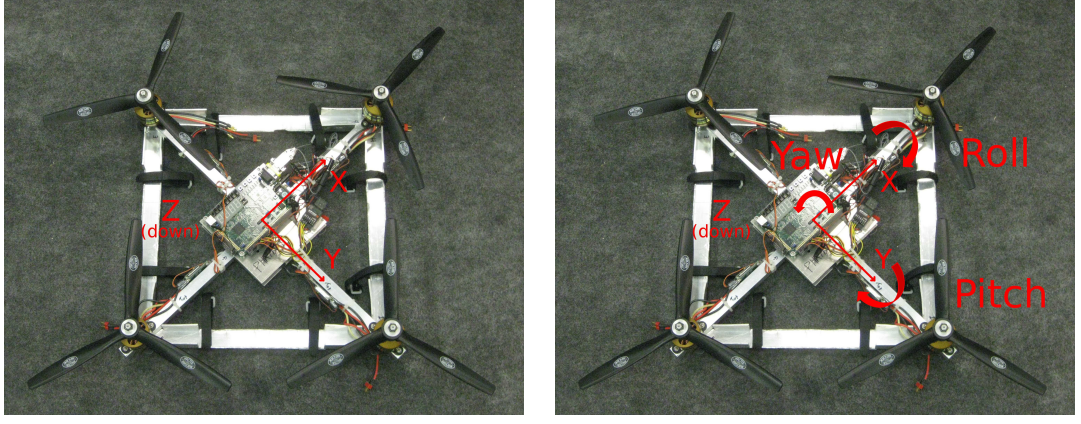
The next step is to generate a simulated flight profile. It is now necessary to include additional vehicle states consisting of the aircraft's roll and pitch angles, along with an altitude.

The necessary state vector to place the aircraft into the simulation at each time a range measurement is taken to generate simulated scans is:

$$\begin{bmatrix} x_b \\ y_b \\ z_b \\ \phi_b \\ \theta_b \\ \psi_b \end{bmatrix} = \begin{bmatrix} \text{X Position} \\ \text{Y Position} \\ \text{Z Position} \\ \text{Roll Angle} \\ \text{Pitch Angle} \\ \text{Yaw Angle} \end{bmatrix}$$

This x, y, and z position are the vector from the original position of the body to its current position. The body frame x-axis points from the center of the body out one rotor. In the case of a quadrotor the nose is chosen by the operator and defined as shown in Figure 3.7(a). The y-axis points out another 90 degrees clockwise when viewed from above, and the z-axis points down to complete a right-handed coordinate frame. Figure 3.7(b) defines rotation about the x axis the roll angle ϕ , pitch angle about the y axis, θ , and yaw is about the z axis, ψ .

3.2.6 Quadrotor Simulator. To provide the best possible results the most realistic flight trajectory was necessary to thoroughly investigate the effects of the dynamics of a flying aircraft on an onboard sensor. This was accomplished through the use of a non linear quadrotor simulator developed at the ANT Center [20]. To simulate a trajectory requires four command inputs for the duration of the flight. These are roll, pitch, and yaw angles, along with a thrust reference for vertical movement. Multiple



(a) Quadrotor Body Frame

(b) Quadrotor Rotation Angles

Figure 3.7: Quadrotor Body Frame and Attitude Angles

flight profiles were produced to fly around the ANT center. These will be detailed in the next chapter.

A typical quadrotor flying with a heavy payload, such as the 360 degree laser scanner, will use angles less than 5 degrees with possible aggressive maneuvers accomplished using angles up to approximately 10 degrees. These rotations of the vehicle will degrade performance of the laser scan measurements as detailed in Section 3.3.2.

3.2.7 Generation of Scans from Flight Profile. The realistic flight profiles of the quadrotor platform provide the capability to detect the effects of flight dynamics on laser scanner measurements. As previously discussed, the calculations generating laser scans require different reference frames. The scanner mounted on the aircraft operates in the body frame, but the algorithms used, (detailed in Section 3.3), operate in the navigation frame. This frame is chosen to be an East, North, Up reference frame. A DCM is used in the transformation of one coordinate frame to the other. The DCM for body to navigation frame is shown in Equation 3.4

$$C_b^n = \begin{bmatrix} \cos(\psi) \cos(\theta) & \cos(\psi) \sin(\theta) \sin(\phi) - \sin(\psi) \cos(\phi) & \cos(\psi) \sin(\theta) \cos(\phi) + \sin(\psi) \sin(\phi) \\ \sin(\psi) \cos(\theta) & \sin(\psi) \sin(\theta) \sin(\phi) + \cos(\psi) \cos(\phi) & \sin(\psi) \sin(\theta) \cos(\phi) - \cos(\psi) \sin(\phi) \\ -\sin(\theta) & \cos(\theta) \sin(\phi) & \cos(\theta) \cos(\phi) \end{bmatrix} \quad (3.4)$$

where ϕ is the roll angle, θ is the pitch angle, and ψ is the yaw angle.

This is used when the scanner finds the range of points in which it would detect and find a range measurement represented by a line segment. This is defined in the body frame as the point of the scanner's position, always $(0,0,0)$, to the point at the range of the sensor when rotated according the vehicle's attitude. To convert this to the nav frame, where the ANT center is defined and measurement occurs, the DCM is first evaluated at the attitude angles of the aircraft, then multiplied to the position in the body frame, and added to the vector between the nav and body frames as shown in Equation 3.5.

$$\begin{bmatrix} X_n \\ Y_n \\ Z_n \end{bmatrix} = C_b^m \begin{bmatrix} X_{b1} \\ Y_{b1} \\ Z_{b1} \end{bmatrix} + \begin{bmatrix} X_{b0} \\ Y_{b0} \\ Z_{b0} \end{bmatrix} \quad (3.5)$$

where X_n is the end point of the laser scan in the navigation frame, X_{b0} is the origin of the body frame and X_{b1} is the end point of the scanner measurement in the body frame

3.3 Histogram Method Calculation

With complete scans available using the above simulation, a method is necessary to extract navigation data. One of the motivations of the histogram correlation method, introduced by Weiss et al., was to develop a navigation method completely independent of odometry for use by mobile robots [42]. Another motivation was that

it be fast enough that it could be used to generate maps in real time so that accumulation of errors would be reduced when returning to a previously mapped location. There were two possibilities this method allowed for this reduction in the accumulation of errors. First, scans that were meters apart are still able to be compared accurately, reducing small error accumulation, and secondly, it was possible that scan matching could correct accumulated error. Adapting these ideas to navigating in a flying environment, where an IMU is used instead of odometry, made this method a primary investigation for a standalone navigation solution or to aid onboard systems.

As introduced in Section 2.4.5 the scan to scan correlation using the histogram correlation method is performed in three steps. First, the rotation angle between the scans is found, then two displacement magnitudes are estimated. This method assumes that a significant portion of the environment is the same, which is typically the case with high scan rates in relation to the vehicle dynamics, so that laser scans can be matched to each other. If inside a non symmetrical room, a laser scan from any orientation and location is theoretically correctly matched to any other orientation and location. In harsher environments additional techniques may allow correct matching through additional knowledge such as vehicle dynamic limits.

The angle determination fits a line between every consecutive point, and calculates the angle of this line and the scanner axis. Parallel walls generate an angle 180 degrees apart and are often combined by current histogram correlation methods. A visualization of how this angle is generated is shown in Figure 3.8. These angles are then placed in a histogram with a selected bin size, which is equal to the smallest distinguishable rotation determined by the algorithm. This is also performed to the second scan and the results placed into another histogram. With no noise on the scanner, and no translation or rotation, these will be identical. If there is only a rotation, these histograms will be identical except for an offset of the angle. A translation will produce different histograms, but with the assumptions that the same walls are visible they can still be compared accurately. To determine the rotation angle between the two scans a discrete circular crosscorrelation is performed.

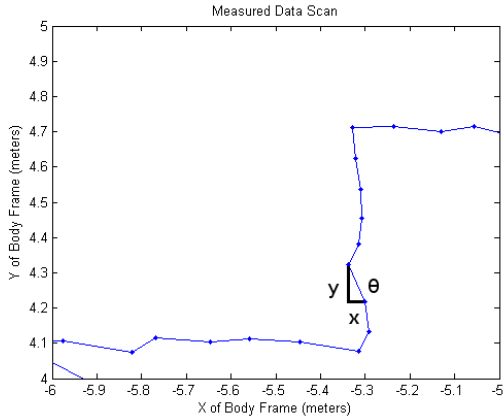


Figure 3.8: Angle Calculation Used in Histogram Algorithm

The maximum of this correlation directly corresponds to the rotation angle θ . Depending on the environment and sensor capabilities, 0.1 - 3 degree bins have proven to provide adequate scan matching. Smaller bins benefit when there is minimal sensor noise and an environment with many points occupying walls facing the same directions. This results in enough data points to create significant spikes in histogram bins.

Upon determination of the rotation angle the scans are rotated on top of each other. The rotation angle determined is subtracted from the angle index for the second scan resulting in overlayed scans with the same orientation. Next, both scans are rotated so that the maximum angle found in either angle histogram, commonly referred to as the "main" direction of the scan or α , is placed upon the x axis. This improves determination of the x and y direction translations between the scans and is especially useful when operating in a man made environment where parallel and perpendicular walls are assumed to exist in the environment. In this thesis the angle histogram was transformed into a 90 degree window where perpendicular walls produce the same angle. The maximum of this was used to rotate the scans by ± 45 degrees.

With both scans rotated to the same orientation, and onto the x and y axis, translation was determined using additional histogram correlations. This time, the x

and y distances between the scanner position and each data point are placed into a distance histogram. While it is possible to use a histogram ranging in size between the minimum and maximum values of the distances, the computational requirement would negate the purpose of the algorithm. The distances are recalculated using the modulo of the distance and the window size selected, setting up a circular correlation to determine translation between the two laser scans. Window size limits the magnitude of the translation that can be detected to half of the window size because of the nature of the correlation performed. Bin size is selected as the minimum resolution of the translation that can be determined. For large translations between scan matches it is common to use two consecutive histogram correlations. The first uses meter sized bins to capture the majority of the translation, which is followed by a second using a smaller bin size to determine the remainder. In this thesis a single correlation for each direction with a window size of 4 meters and bin size of 1 cm allow translation determination up to 2 meters to the nearest centimeter.

The histogram correlation algorithm as used for this research is outlined as follows:

1. Calculate angle histograms of both scans
2. Correlate first and second scan angle histograms to determine rotation angle θ .
3. Determine the highest occurring angle in scan 1 (α).
4. Rotate scan 1 by α
5. Rotate scan 2 by $\alpha + \theta$
6. Create histogram for distance of each point to the x axis using 1 cm bins
7. Correlate for Δx
8. Create histogram for distance of each point to the y axis using 1 cm bins
9. Correlate for Δy
10. Transform body translation to navigation frame by using the sum of magnitudes in each of the x and y directions and current heading angle found by using previous heading $+ \alpha$

A visual representation of matching two scans is found in Figure 3.9. Two scans taken in the ANT Center are shown in the top left. The scanner position of all scans

in the body frame is (0,0). The angle correlation calculates a heading change (θ) of -4.1 degrees which is added to the second scan and shown in the top right. Bottom left shows the scans after rotated by the main direction (α). The algorithm then calculates a Δx of 10 cm, and a Δy of 56 cm. The successful matching is shown in the bottom right.

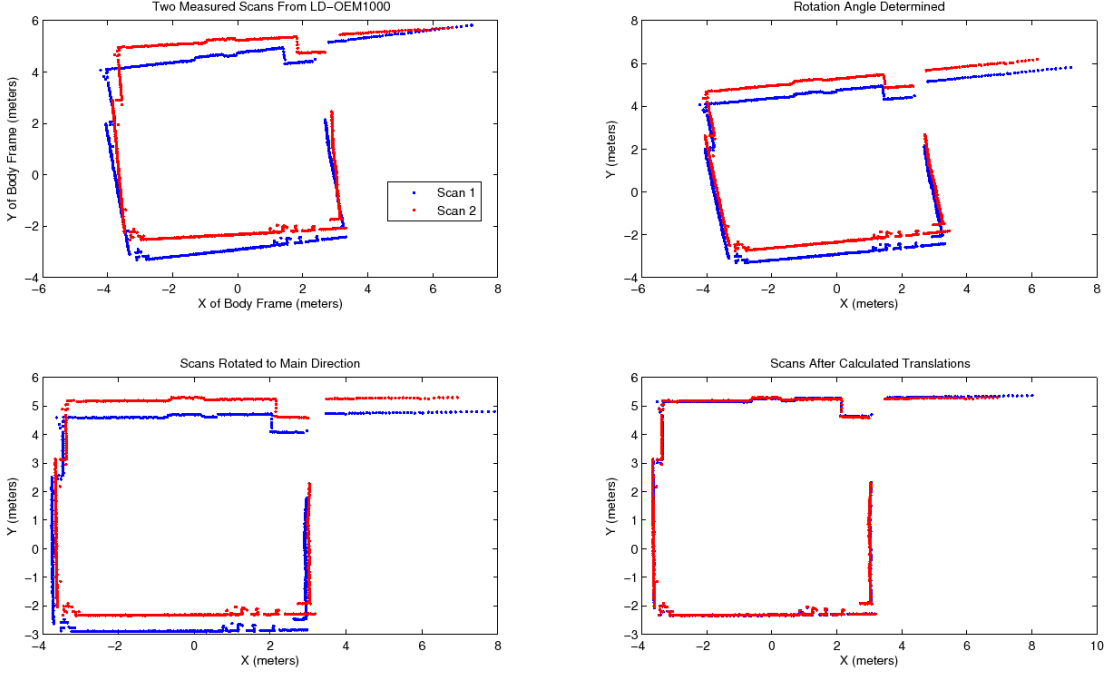


Figure 3.9: Histogram Correlation Method Matching Two Scans Taken in the ANT Center

This algorithm is robust to elements including objects moving through the laser scanner area and some sensor noise. However, it does not always determine a single value for the maximum correlation. When this occurs the result is not appropriate to include as an update. Using this method allows the next scan to be used without any significant impact in performance as long as the limits are not surpassed, (such as a translation greater than two meters described in this application). This may cause stability issues if a poor scan is not handled properly and cannot be matched to any future scans. Additional challenges to the algorithm in the ANT Center environment include the interior walls are not straight as they are built of individual sections about three feet long. These walls prohibit the LADAR to observe the entire ANT Center

at anytime from any position. Also, transitioning into the hallway and back produces a significantly different viewable environment. The algorithm should handle these challenges suitably.

3.3.1 Extraction of Vehicle Movement. The histogram correlation algorithm resolves scan to scan movement in the body frame, as a heading change, and an x and y translation. To convert this into the navigation frame a DCM must first be applied in two dimensions shown in Equation 3.6.

$$\begin{bmatrix} x_n \\ y_n \end{bmatrix} = \begin{bmatrix} \cos(\psi) & \sin(\psi) \\ -\sin(\psi) & \cos(\psi) \end{bmatrix} \begin{bmatrix} x_b \\ y_b \end{bmatrix} \quad (3.6)$$

The vehicle is assumed to have no pitch or roll angles when performing this transformation as the quadrotor's limited pitch and roll angles can use the small angle approximation where the cosine of small angles is very near 1. For example, if ignoring the y direction, the quadrotor travels 10 cm at a pitch angle of 2 degrees the true movement is 9.994 cm in the x direction and 0.35 cm in the z direction as detailed in Figure 3.10. Also, the algorithm is more likely to estimate incorrect movement based upon skewing range measurements, as detailed in Section 3.3.2, rather than acquiring error due to these small cosine effects. The calculated x and y vectors in the navigation frame are added to the previous estimated position to determine the new current position.

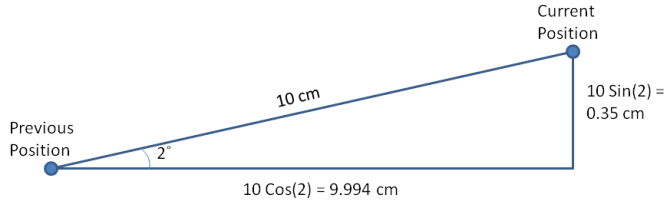


Figure 3.10: Quadrotor Operation uses Small Pitch and Roll Angles Allowing the Application of the Small Angle Approximation

This histogram correlation method uses relative positioning meaning any heading and position is relative to its first known (or assumed) state. The total translations are continually integrated over time. A faster update rate will cause an increase in the accumulation of the small errors to grow over time, but too slow of an update rate may fail when the environment changes too quickly such as passing through a doorway with limited visibility through either direction. Updates rates of 10 Hz, 5 Hz, and 1 Hz are examined in both simulated and experimental trials.

An acquired heading error will continually impact the x and y errors as the calculated values will not coincide with the x and y axes of the navigation frame. Overall, error growth of this method can be attributed primarily to rounding errors and incorrectly selected correlations, which are caused by sensor noise or environment anomalies, and also constant rounding of translations and angle to the bin size available.

3.3.2 Flight Attitude Effect On Range Measurement. As the quadrotor maneuvers in flight, the distance determined by the scanner changes depending on the orientation of the vehicle. As a stationary vehicle rotates either direction away from horizontal the same wall will appear to move away from the laser scanner as depicted in Figure 3.11. This effect is greater the further from a wall, and the larger the angle changes between scans as shown in Equation 3.7.

$$\text{Measured Distance} = \frac{\text{True Distance}}{\cos \theta} \quad (3.7)$$

The effects of this when operating in the assumed environment and accounting for the limited attitude angles during quadrotor operation result in changes of approximately 10 cm in the worst case. These effects will be analyzed in Chapter 4 comparing two and three dimensional simulations. When an onboard INS solution is available the effects of this can significantly reduced as a measured scan can be scaled according to pitch and roll angles.

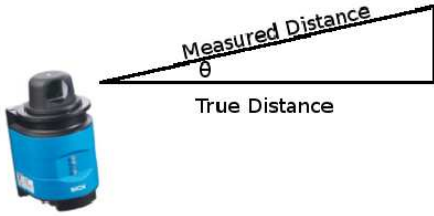


Figure 3.11: Scanner Measurements are Greater than or Equal to the True Distance to the Wall

3.3.3 Application of a Smoothing Filter. When the histogram method was first applied to both the simulated and truth scan, the first step of determining rotation angle was not performing well to the desired accuracy of 0.1 degrees. The reason for this is the noise associated with the scanner caused the angle calculation to struggle. Consecutive points on walls are assumed to have similar angle, but as shown in Figure 3.12, this did not provide the ability to correlate scans as the angle histogram would have a maximum of 3 or 4 hits for any bin of 0.1 degrees. This is partially caused by operating the scanner at a high resolution near objects where many measurements occur near each other. A moving average filter was applied which averaged between 1 and 20 consecutive points in an attempt to smooth the noise effects on the scan so the histogram would have more defined peaks where the walls occur. This method would be ideal for an environment without any objects except for the walls. Through this method the effect shown in Figure 3.12 is improved as seen in another scan found in Figure 3.13(a). In the case of a single measurement located away from a wall the filter will not smooth noise, but instead shift the group of points first toward the object and then back. This effect is detailed in Figure 3.13(b).

Initial determination of the optimal filter length observed a single scan at a time along with its associated angle histogram. Without filtering there were no significant

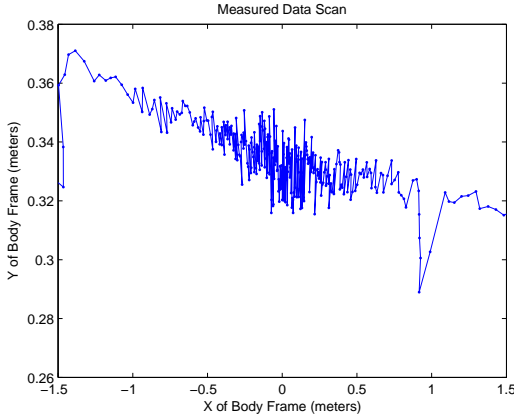
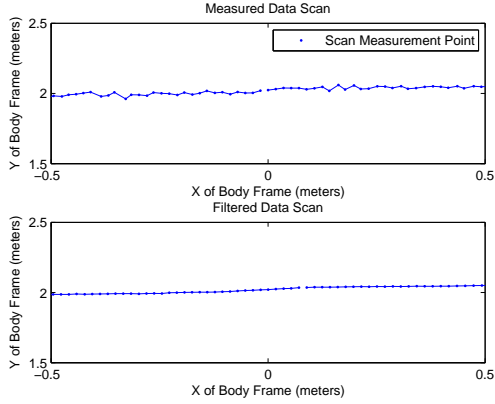


Figure 3.12: Laser Scan Produced when Operation a Laser Scanner Near a Wall

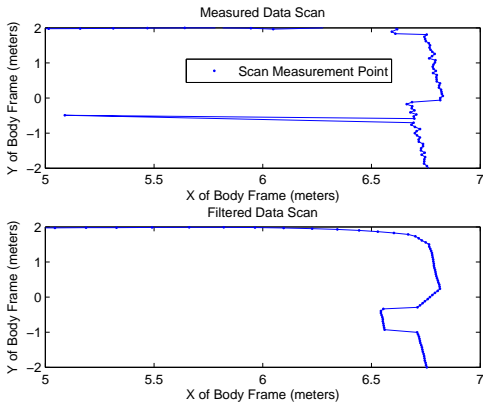
spikes which would cause the algorithm difficulty in determining the correct rotation between two scans. Out of 720 measurements occupying 3600 bins, the maximum value in any bin was 3. Increasing the filter setting made individual walls visible. While not all points occupied the same 0.1 degree bin, there were a few consecutive bins with high results. In the ANT Center the maximum values ranged between 15 and 20 depending on the location in the room when applying a filter length of 15. Increasing the filter setting beyond 20 reduced the spikes as significant portions of walls were mixing with adjacent walls. Additional details of filter setting analysis are found in Chapter 4.

3.4 Line Extraction

Another method commonly used to extract information from laser scans or vision cameras is through the use of a line extraction algorithm. Using the assumption that the laser scanner is operating in a man made environment will provide many opportunities of straight lines to be found in the laser scan whether they occur inside a room, in a hallway, or even the exterior of buildings. There are many different extraction methods with a few compared using a SICK LMS-291 by Nguyen et al. [31]. This technique is most often applied to SLAM applications where landmarks are tracked over time.



(a) Operation of the laser scanner near a wall produces many points where angle calculations are irrelevant. Smoothing reduces these effects.



(b) When there is an object located away from the wall, the wall becomes skewed. This effect degrades performance the most when it occurs near a corner.

Figure 3.13: Filtering the Scanner Data Provides both Good and Bad Effects

The Hough Transform is a technique whose name is from Paul Hough who patented the idea in 1962 [13]. It is used in image processing to detect lines through a voting process. The lines are represented by two parameters, a distance of the vector from the origin normal to the line, ρ , and the angle of this vector to the origin's axis, θ , as shown in Figure 3.14. Equation 3.8 represents the equation of a line in Hough space using this notation.

$$x \cos(\theta) + y \sin(\theta) = \rho \quad (3.8)$$

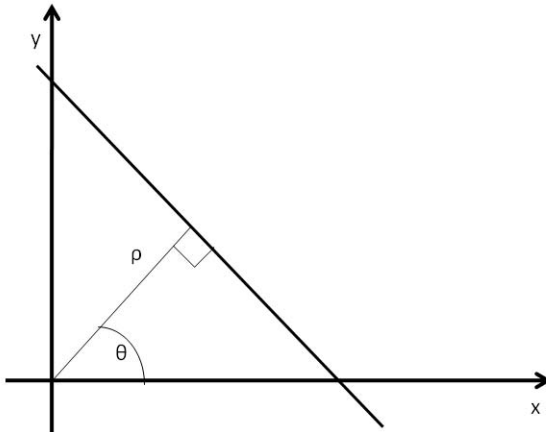


Figure 3.14: Hough Space representation: ρ, θ

This technique of representing lines is used by the line fitting algorithm used by the CAS toolbox for MATLAB [3]. This toolbox is specifically designed for use with laser scanner range data. A single scan where line extraction is performed is shown in Figure 3.15. This algorithm is detailed as follows:

1. For every portion of points using a sliding window across the range readings
 - (a) Fit line model to points within window using least squares estimate
 - (b) Calculate model fidelity measure
 - (c) If model fidelity satisfies condition, create a segment out of this line
2. For all line segments found
 - (a) Check if each pair of line segments are collinear and satisfy a significance level(α)
 - (b) Fuse collinear segments into a line

This method is investigated as an alternative to the histogram matching algorithm. Results are included in Chapter 4.

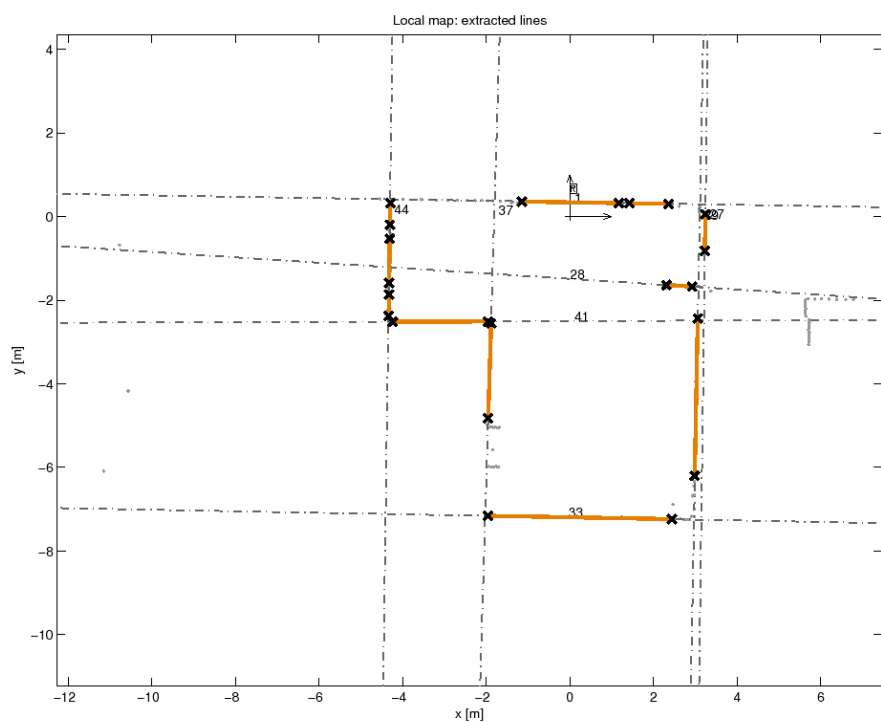


Figure 3.15: Extracted Lines of from an LD-OEM 1000 Range Scan of the ANT Center

IV. Performance Analysis

This chapter reports on the performance of the algorithms used both by MATLAB simulation as well as processed data scans using collected laser scan measurements from an LD-OEM 1000 laser scanner.

4.1 Simulation Results

By developing a simulation to model quadrotor flight, the resulting laser scans that would be measured, along with the processing of these scans, the various effects of each step can be isolated to measure performance characteristics. Monte Carlo simulations of each setting are performed to observe the average effects over many trial runs. A number of 25 was selected for all trials to capture the general trends and results without the burden of extreme computational resources and time. For each trial run the simulation is provided with the perfect scan measurements for the selected flight profile assuming there is no noise on the measurement, and no error in the angle of which the measurement is being taken. Noise is then added as specified by the current simulation variable setting. The measures of performance for each trial are the error in the x and y direction and heading angle. Across all trials the performance is evaluated using the statistical measures of the mean and standard deviation of the magnitude in the X and Y directions along with the heading angle across all points of the simulated run.

4.1.1 Flight Profiles Used in the Simulation. Various flight profiles were generated to analyze the performance. Profile 1 is a 44 second long flight generated as a possible flight trajectory where a quadrotor navigates around a room, then returns to the original location. A detailed view of the required command inputs are shown in Figure 4.1(a) and resulting profile is shown in Figure 4.1(b). A top down view of this as flown in the ANT Center is shown in Figure 4.2(a). Profile 2 is generated by taking the reverse of Profile 1. The last step of Profile 1 is identical to the first step of Profile 2 and the opposite trajectory is found. This assumption is valid because a pitch used in Profile 1 to slow the velocity in a direction becomes a pitch to increase

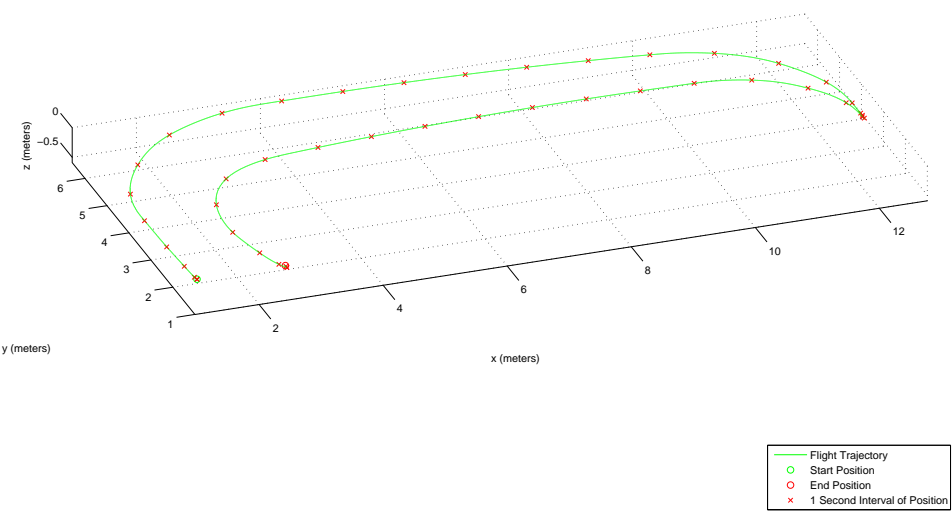
the velocity in the opposite direction of Profile 2. Also, because the quadrotor is near stationary at the beginning and end these can be viewed as independent flights. Profile 3 is identical to Profile 1, but shifted 3 meters in the x direction so that the quadrotor flies into the hallway before returning as shown in Figure 4.2(b). This aids in the investigation of the degradation in performance of the vehicle moving to a dissimilar area. Profile 4 is the opposite of Profile 3, generated using the same method as Profile 2.

4.1.2 Simulated Noise Levels. In addition to changing the flight profile, the simulation was tested across various noise levels on the scanner measurement. As shown in Section 3.2.3 the expected noise level of the scanner was to be a Gaussian noise around the true distance with a standard deviation of 3.8 cm. A noise level of 2 cm, and no noise, were all processed to investigate how this would affect the position and heading calculation.

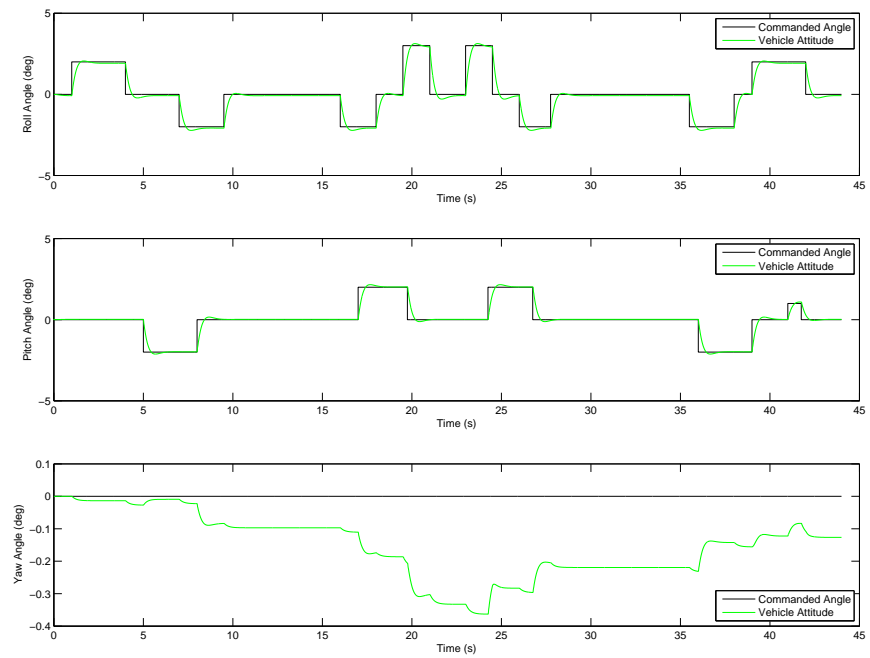
4.1.3 Update Rate Analysis. There are advantages to altering the update rate of this algorithm. A slower update rate benefits in that the small accumulation of errors that occur every time data scans are correlated by rounding to the nearest centimeter are minimized slowing the error growth over time. However, if updates performed too fast and the vehicle flies through a doorway and experiences a dramatically different scene the correlation process may fail resulting in an erroneous navigation solution. The simulation was tested at rates of 10, 5 and 1 Hz to investigate these hypotheses. Figure 4.3 confirms the hypothesis that a slower update rate provides a more accurate solution. Both 1 and 5 Hz perform similar, and better than the 10 Hz and their simulation runs are more tightly around the truth as shown by the standard deviations. Next, Profile 3 was used to investigate performance when flying through a doorway. These results are shown in Figure 4.4 and show poor performance at the 1 Hz rate. The errors in these simulations were not tied to traversing the doorway, but occurred at 8 seconds into the profile which is when the vehicle traverses through the middle of the room. Although the position was not correct, the heading angle

still performed well as it is independent of the translation. Translation, however, does depend on an accurate heading.

Figure 4.5 provides details into each run of the Profile 3 simulation when scans are processed at the previously mentioned rate of 1 Hz, and an averaging filter size of 10. The performance in the X direction is very poor without any runs determining the correct translation. As the scans are matched at 9 and 10 seconds none of the 25 trials estimates a correct translation (within rounding error) shown by the significant jump in the magnitude of the error in all cases. However, in some cases the Y direction is successfully calculated.

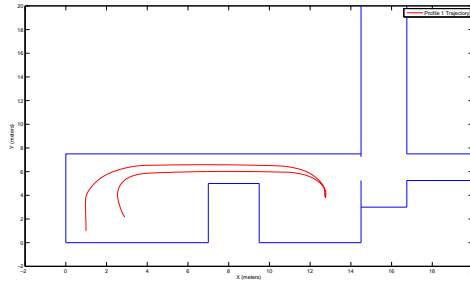


(a) Profile 1 Flight Trajectory

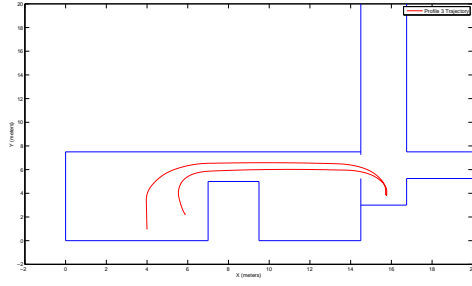


(b) Profile 1 Commanded Attitude Angles

Figure 4.1: Profile 1 Simulation



(a) Profile 1 Flight Trajectory as shown Inside the ANT Center



(b) Profile 3 Flight Trajectory as shown Inside the ANT Center

Figure 4.2: Top Down View of Simulation Profiles Inside the ANT Center.

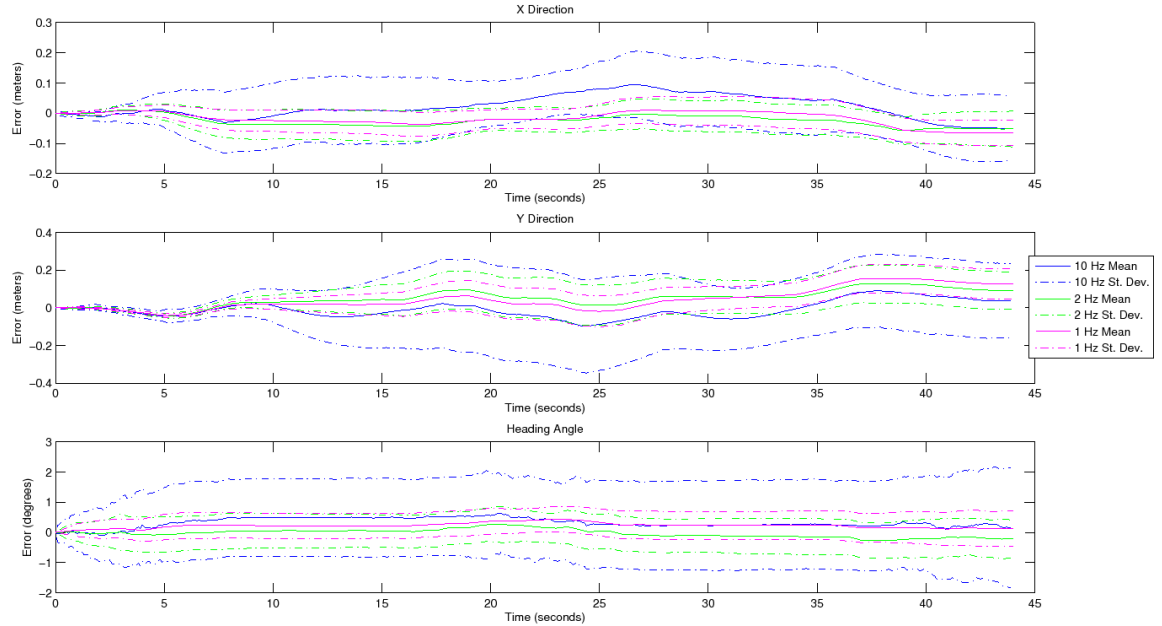


Figure 4.3: Comparison of Update Rates for Profile 1, Noise of 2 cm, and Filter Setting of 10

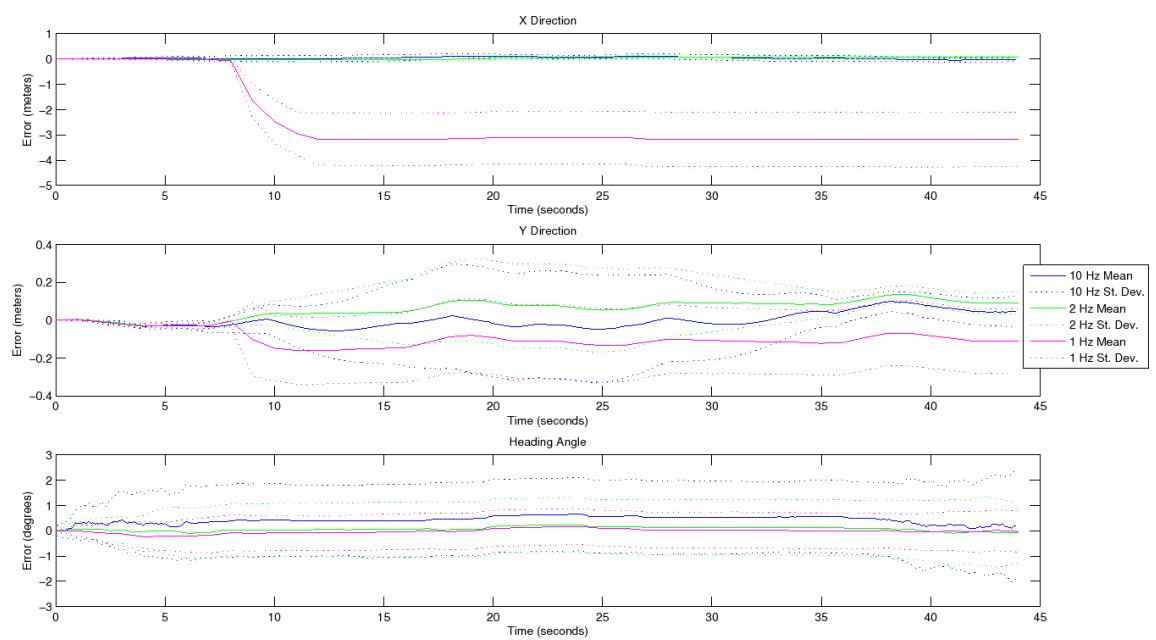


Figure 4.4: Comparison of Update Rates for Profile 3, Noise of 2 cm, and Filter Setting of 10

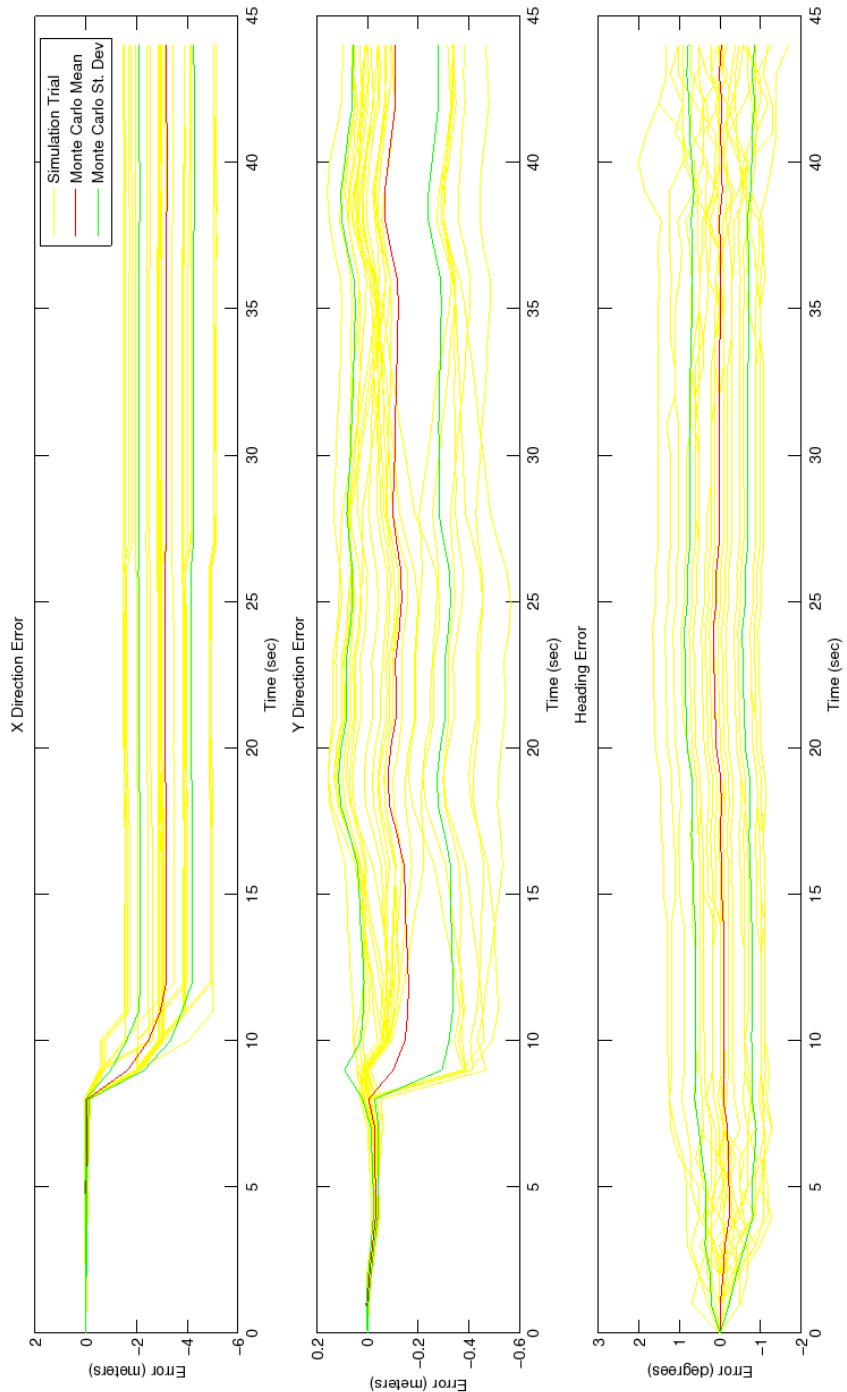


Figure 4.5: Monte Carlo simulations showing poor performance at an update rate at 1 Hz

4.1.4 Smoothing Filter Selection. The simulation assumes a clutterless environment where only walls are found by the laser scanner as previously described in Section 3.3.3. While some filter was proven to be necessary, the optimal window for a moving average was evaluated using multiple techniques. The specific profile primarily used in this investigation was Profile 3, at a noise level of 2 cm, and an update rate of 10 Hz. These errors were quantified by analyzing the statistics of the X and Y error and standard deviation at the end of the simulated profile, along with the average X and Y error and standard deviation across the entire run. A selection of these which changed the most and showed differing performance are shown in Figure 4.6.

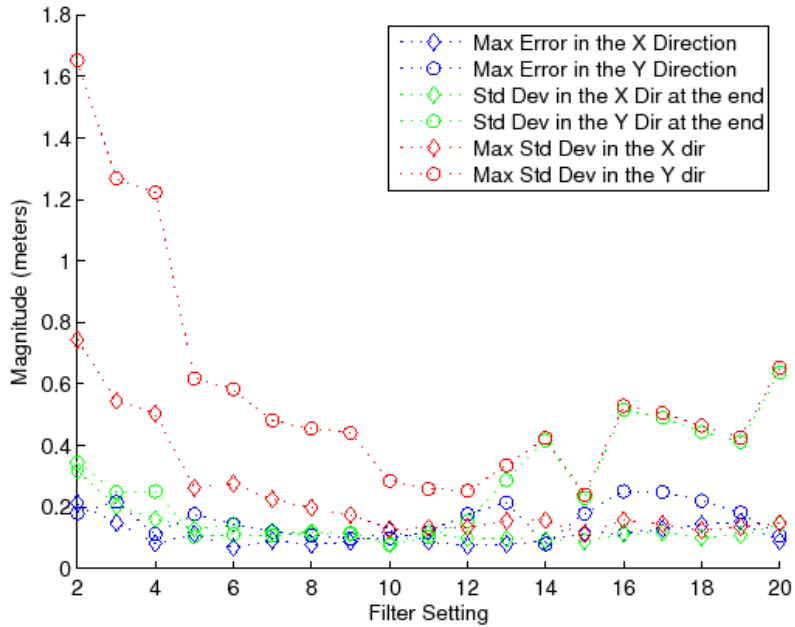


Figure 4.6: Filter Selection Method using Statistics Across Profile 3 Simulation Trials

Each individual trial is plotted against each other with the mean errors shown in Figure 4.7. The low filter settings tended to underestimate the X direction while the rest of the settings performed similarly. In the Y direction the low settings performed the worst with the rest intermingled. The standard deviation results provided more useful results and are found in Figure 4.8. For both directions a low filter setting results in a large standard deviation due to picking up a heading error throughout the run which greatly impacts the algorithms accuracy to compute X and Y translation

correctly in the navigation frame. The average and standard deviation of errors in heading calculation are shown in Figure 4.9. As expected, the average across Monte Carlo trials perform relatively well, however the standard deviation shows how each trial results in a significantly different navigation solution. To compare Figures 4.10(a) and 4.10(b) show the 25 estimated paths for the filter settings of 5, and 15. Both are able to estimate the approximate trajectory, however the setting of 15 is much closer to truth.

From this evaluation in simulation it is estimated that the best filter would be at a setting between 10 and 15. Results from the experimental data are found in Section 4.2.

4.1.5 Comparison of 2 and 3 Dimensional Simulation. By comparing two and three dimensional simulations the immediate degradation in performance by introducing roll and pitch angles can be analyzed. The simulated laser scans for the two dimensional environment used only the x and y position, and the heading of the vehicle. The rest of the vehicle state vector was ignored and the scans were generated using the two dimensional line segment intersection method. For the three dimension environment the other vehicle states: roll, pitch, yaw, and altitude, are included causing the scans to skew and change as detailed in Section 3.3.2. While most of the simulated profiles showed some loss in performance overall results showed the these effects not to severely hinder the performance of the algorithm in this setting. A few examples of the comparison between 2 and 3 dimensional performance are shown. First, Figure 4.11 is the performance of Profile 4, with a noise setting of 4 cm, processed at 10 Hz, and a filter setting of 15. The general trends in error growth are very similar with the average errors often coinciding. However, the standard deviation shows that the 3D simulated results are more spread out than the 2D case, especially towards the end in the Y direction. Another example shown is Figure 4.12, is profile 1, with a noise level of 2 cm, processed at 10 Hz, with a filter setting of 10. Again these perform similarly with the 3D having a larger ending standard deviation.

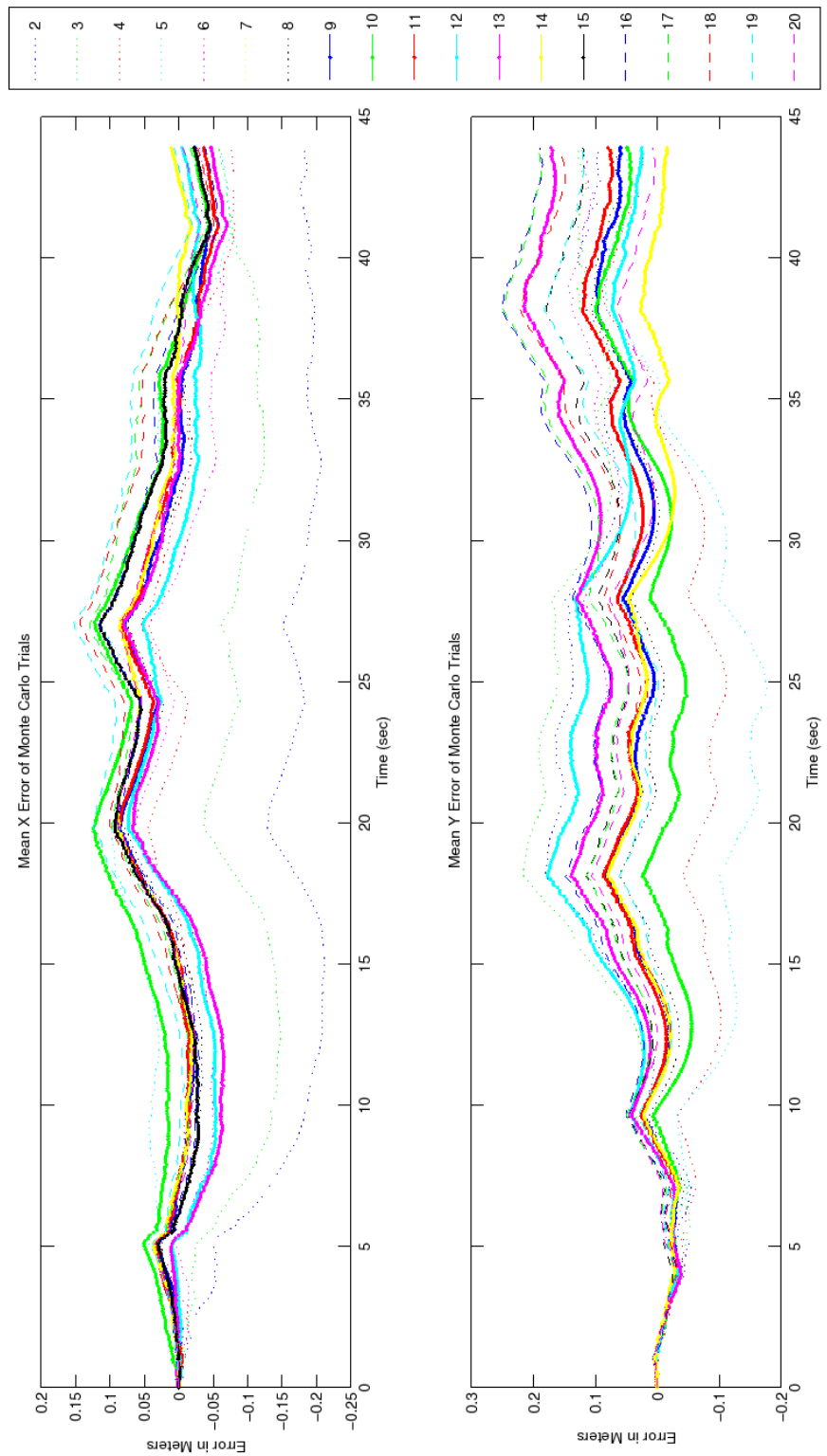


Figure 4.7: Mean Error in X and Y Direction

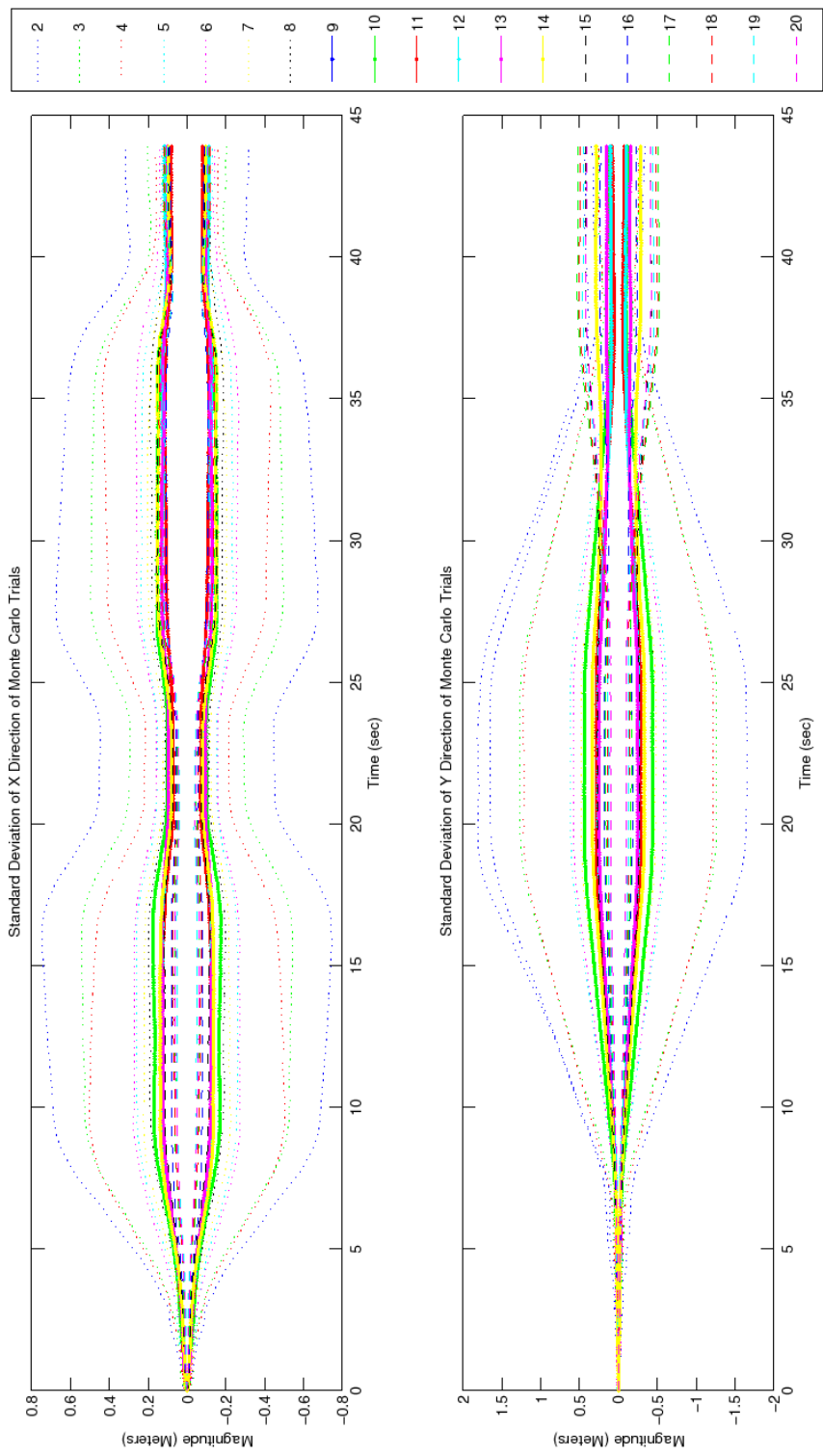


Figure 4.8: Standard Deviation of Error in X and Y Direction

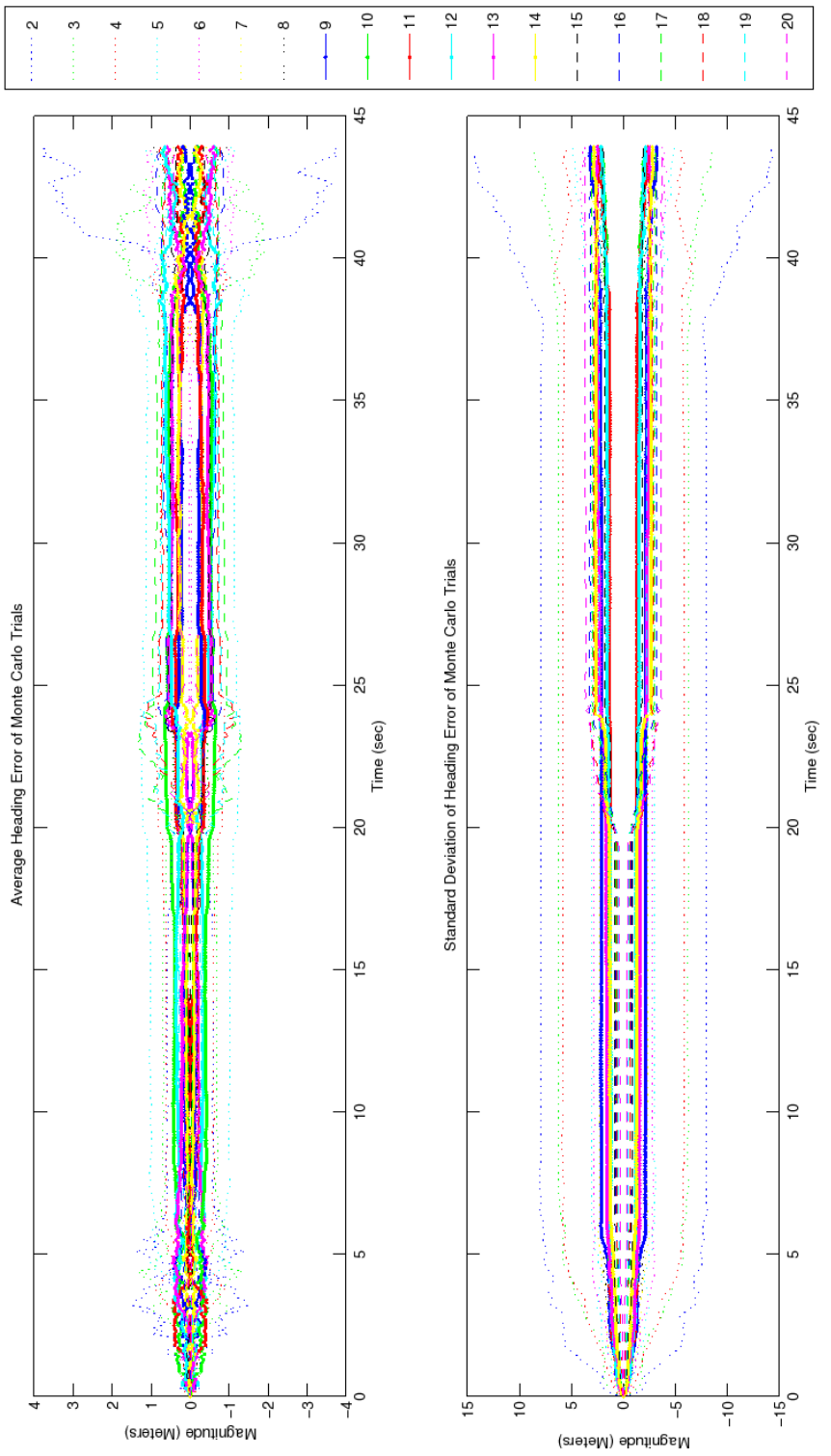
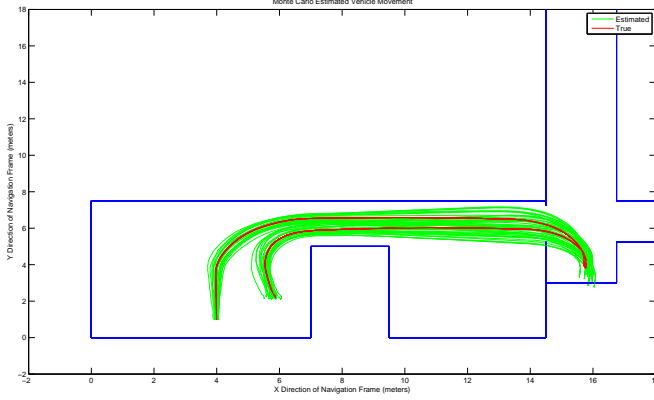
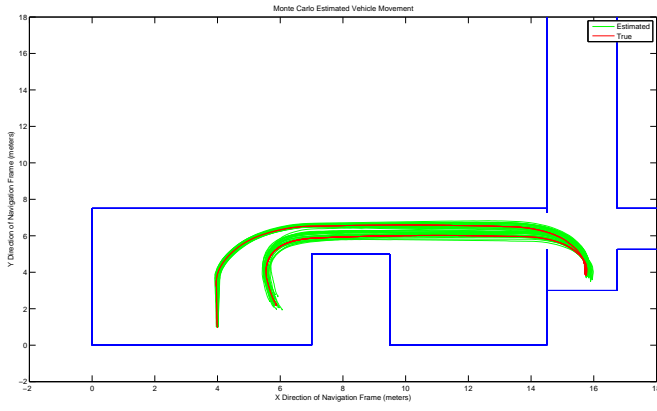


Figure 4.9: Heading Mean Error and Standard Deviation



(a) Estimated Trajectories with Filter Setting of 5



(b) Estimated Trajectories with Filter Setting of 15

Figure 4.10: Filter Setting

4.1.6 Extended Length Simulation Testing. Characterization of the error growth using the histogram correlation algorithm over a long period of time is of great interest. Ideally, bounded growth in any estimation scheme is desired as operation over long periods of time, even many hours, results in the same uncertainty of measurements, as is the case with GPS. Using Profile 1 followed by Profile 3, and again repeating Profiles 1 and 3, created a simulation of four times the length of the original profiles. By comparing the error growth rates in this situation provides insight into overall error growth using this method. These are found in Figure 4.13 and show the results of processing the longer profile at 10 Hz, at a noise of 2 cm, and a filter setting of 15.

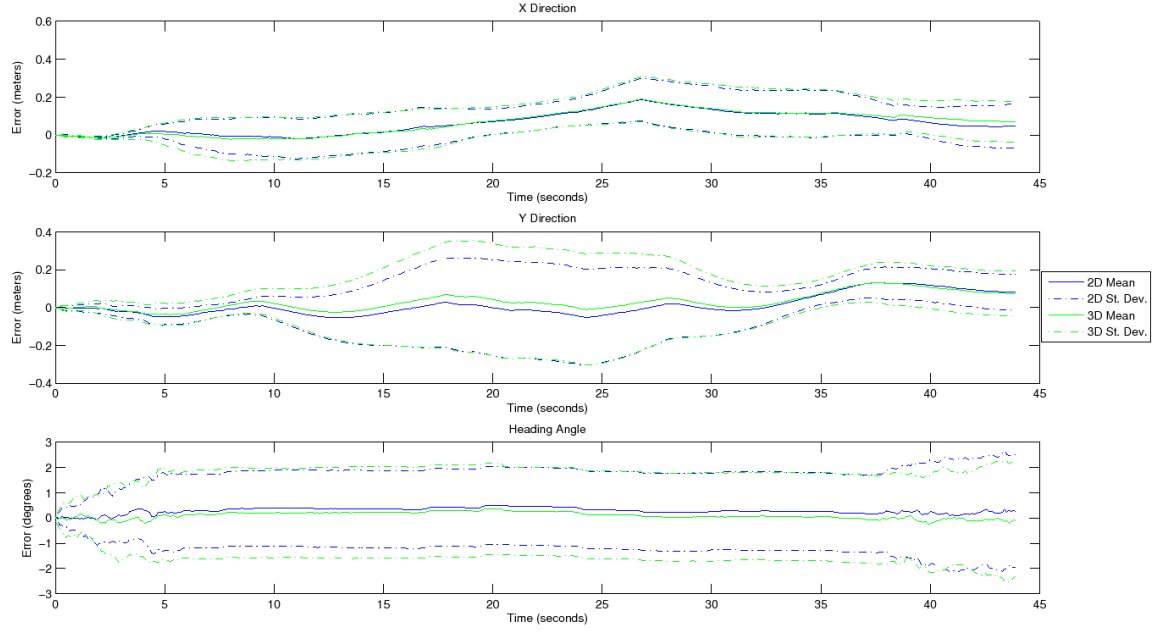


Figure 4.11: 2 D and 3 D Comparison of Simulation Profile 4

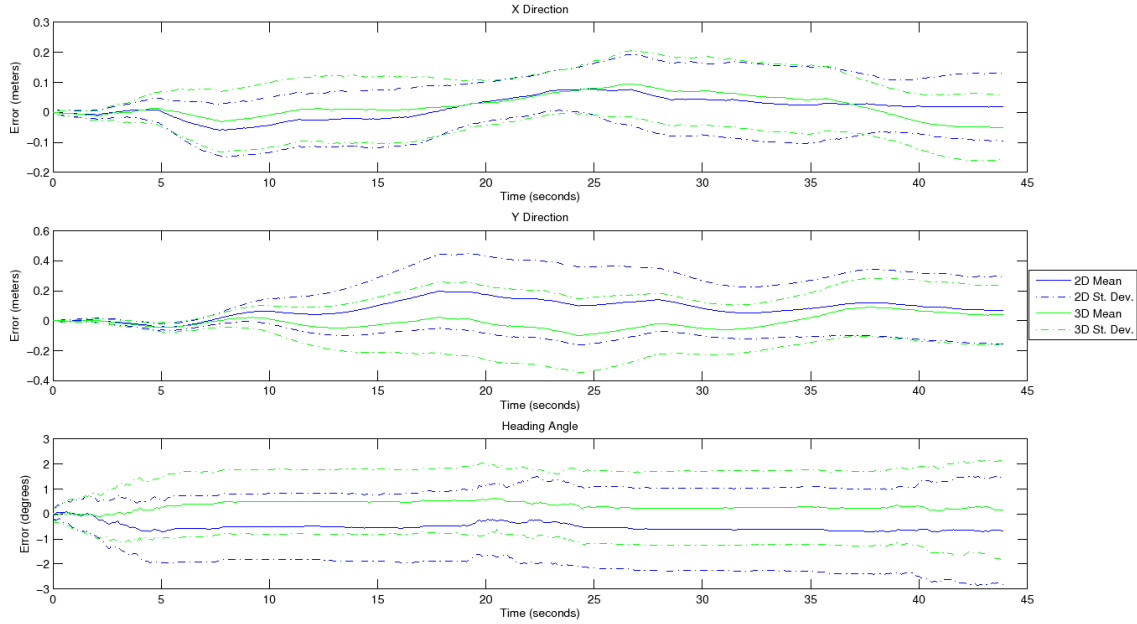


Figure 4.12: 2 D and 3 D Comparison of Simulation Profile 1

These results indicate that performance of the algorithm is trajectory dependent. This is shown by the periodic growth and decay of the standard deviations in the errors according to what portion of the profile is being flown. Overall, the average X

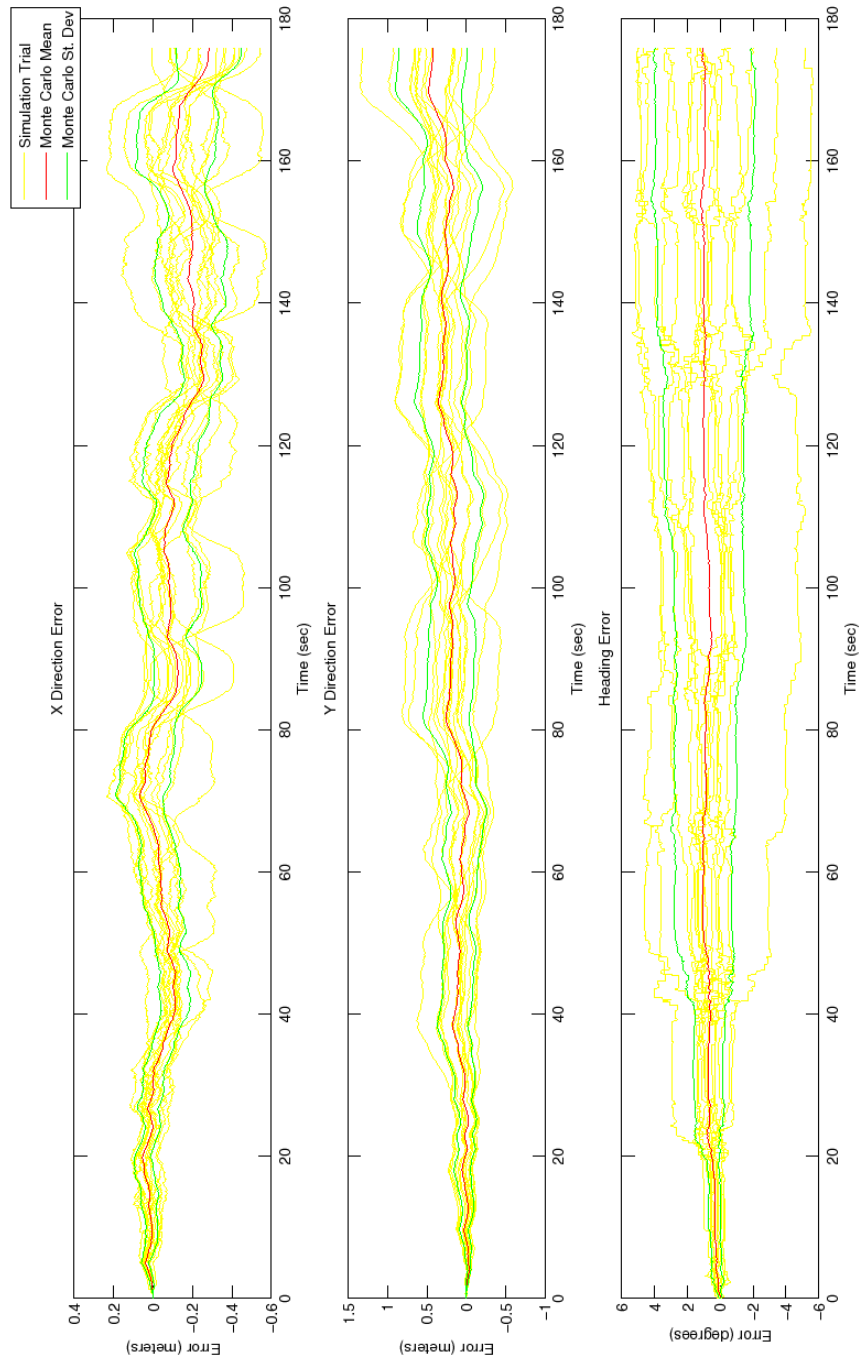


Figure 4.13: Error Growth of A Longer Simulation Profile

position error after 3 minutes and 56 seconds was determined to be 28.29 cm with a Y position error of 42 cm. This is a total positioning error of 50.1 cm. The average heading angle error at the end was 1.03 degrees. Although the standard deviations

of all errors tend to be influenced by the vehicle trajectory, they do grow over time. An approximate numerical analysis of the error growth in the simulated environment would be an average error in both X and Y direction of 10 cm per minute each, with an uncertainty growth of ± 15 cm per minute. The error growth in heading angle determination is one degree per minute with an uncertainty of ± 2 degrees per minute.

4.2 Experimental Results

4.2.1 Device Setup. Data was collected in the ANT Center by interfacing with the LD-OEM 1000 with the SICK LIDAR Matlab/C++ Toolbox [11] either through an RS-232/422 serial connection, or over Ethernet. The LMS series of SICK laser scanners use serial while the LD series uses an Ethernet connection. This toolbox allows setting the measurement sector(s) of the field of view for the scanner, angular resolution, and others, but the driver program for Windows provided by SICK was used during setup of the device.

The LD-OEM 1000 provides range and reflection measurements, time tags, and the angles at which the measurements were taken by providing the start and end angles along with the angular resolution. A collection of data using the settings used in these experiments of a full 360 degree scan, at a resolution of one half degree, and at a rate of 10 hz. Hundreds of consecutive scans were saved using Matlab. When analyzing this set of data it was determined that there were dropped frames for unknown reasons. This was verified by looking at the beginning and end time stamps associated with each data set and appeared at random intervals across the entire data collection. The average data rate of the collection with dropped frames was between 9 and 9.5 hz. This effect is shown in Figure 4.14. Without dropped frames each scan would start every 100 ms, but gaps of 200 ms can be seen. To minimize the chance of this happening, everything to reduce the computational requirements was implemented in attempts to resolve this. Even without collecting reflection measurements, removal of all messages displayed in the Matlab command window, and preallocation of memory for the data scans had no affect on the missing measurements.

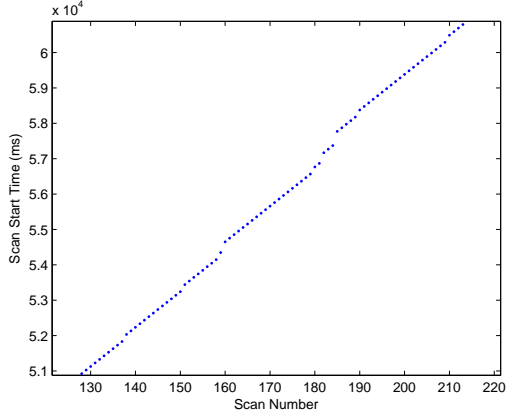


Figure 4.14: Beginning Time Stamps of LADAR Measured Data show Dropped Frames

While the goal is to use the data in real time, the data scans were post processed allowing individual datasets to be processed multiple different ways to compare performance. Update rates of 10 Hz, 2 Hz, and 1 Hz were compared by using every scan for a 10 Hz update rate, or in the case of 2 Hz, using every fifth scan. When possible, the time tags were also used to pick out the appropriate scans. When a dropped frame was desired, the next available scan was used instead. These data scans were also processed using various smoothing filter values of between 0 and 20. Anything above this was decided to be unnecessary and likely to degrade performance as large portions of true walls would become skewed.

4.2.2 Realtime Data Display. The histogram correlation method was implemented in real time where movement in the body frame is displayed using MATLAB. Doing so creates an easy method to observe certain phenomena such as people walking through the room or testing limits to the rate of movement necessary to be detected. While the algorithm is fast and should be capable of running at the 10 Hz scan rate of the device, this was not quite achieved. It's possible this was due to the timing of the scans being available, the processing time involved, non-optimized code, and the overhead of outputting the results to the display. The most probable reason for not achieving 10 Hz is the small bin sizes used in the histogram correlations of a

tenth of a degree for angle, and 1 cm for each translation bin. This contributed to a much larger processing requirement than previously demonstrated by others using the method [42]. An update rate of 5 Hz used every other scan of the device operating at 10 Hz. The higher scan resolution is desired as interscan movement is minimized which degrades the scan quality. The realtime display was able to confirm that the algorithm is robust when people walk through the scanned sector, even when fairly near to the scanner obscuring vast portions of the scan. This is because the person only distorts a portion of one or few walls in a scan. The remaining portions of the wall will still result in a successful correlation, just not as strong.

Another concern when applying the algorithm to real scans was a small but constant rate of change in heading. This was investigated as a possible error source because the scan may become distorted rather than the algorithm detecting a rotation change. This concern was not observed when analyzed with realtime data. Conversely, the x and y translation did not perform as well when introducing a similar small, but constant movement. To overcome this a reduced bin size may be necessary. However, this error source is platform dependent and restricted to a vehicle expected to spend a duration time in a hover. This will not be a primary concern during the operation of this method on a quadrotor.

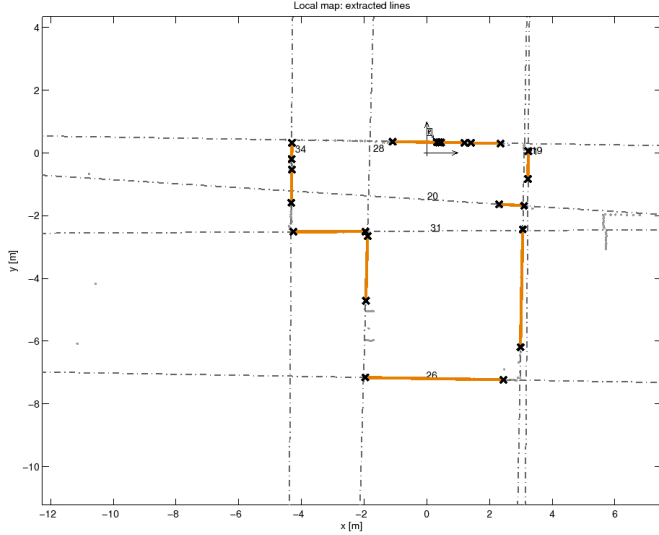
4.2.3 Experimentation using Line Extraction. In order to compare performance to another common method, the line extraction method detailed in Section 3.4 was implemented using true data scans from the ANT Center. Extraction of rotation and translation is possible using this method by using a search window for each line found between two consecutive scans. By using the angle to each line, and the distance to the point normal to the line, rotation and movement could be extracted similar to the rotation and two translation idea as used in the histogram correlation method. This method is more common to implement when using SLAM.

Two consecutive scans taken with the LD-OEM 1000 were compared to investigate the algorithms performance. The resulting lines fit to the scans are found in

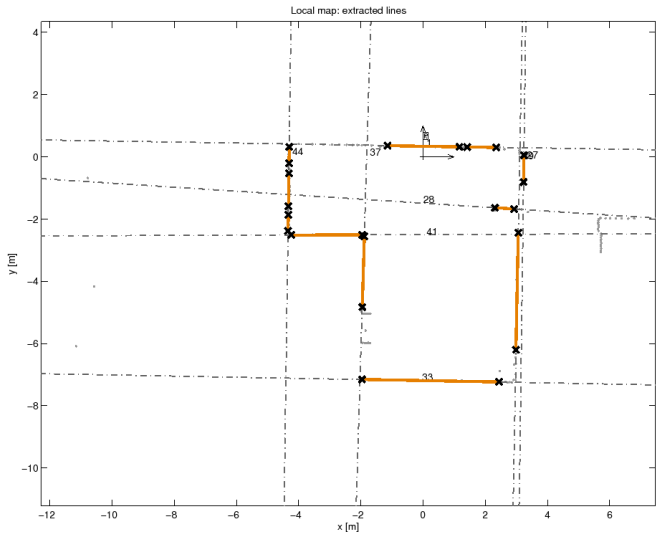
Figures 4.15(a) and 4.15(b). Each segment found is displayed as a line with an x for endpoints. These segments are then joined into lines shown by the numbered and dashed lines. The laser scan data points are shown with a single gray dot. The algorithm performed quite well using default line fit parameters and tolerances of joining segments to lines. The top wall, nearest the scanner origin, fits a single line to 3 line segments. Most of the exterior walls of the ANT Center were fit to a line, along with a line found for the door which was propped open.

Results of the accuracy of this method provide promising results for use in navigation. Hough representation of corresponding lines in these scans were fit within an angle, α , of 0.2 degrees and distance, r , of less than 1 cm. This method was determined to take too long, requiring over a half second processing on each scan when using a desktop computer, and was not beneficial for the purpose of an onboard immediate solution so it was not investigated further. Computation time was problematic due to the amount of data points required to be processed. A line segment was fit to every consecutive window of a user specified number of points before fitting these segments into lines. For this method to perform faster the resolution of the scanner could be lowered to reduce the number of line segments fit or to increase processing power.

4.2.4 Data Collection. After initial interfacing with the laser scanner and applying the basic algorithms to experimental data, a method for moving the device was developed to investigate performance. The device was mounted on a moving cart, shown in Figure 4.16. This was rigidly mounted and does not allow for simulated pitch or roll angles, but it provides the opportunity to use real data from a realistic, yet cluttered, environment. To measure performance, a truth data source, or at least a method which is proven to provide an order of magnitude better measurements, is necessary. Initially a Novatel SPAN IMU HG1700 was used for its high rate of measurement and expected accuracy especially over such a short test run. It was initialized using dual stationary GPS antennas, however, after disconnecting and traveling paths inside the ANT Center and surrounding hallways the position solution



(a) Scan 1



(b) Scan 2

Figure 4.15: Two Consecutive Laser Scans in the ANT Center with Extracted Lines

was not reliable. The IMU was taken down a 25 meter hall way and returned to start, but was off by more than 5 meters and was unable to be used in any comparison. Additional processing may resolve issues such as misalignment where the IMU was not sitting horizontal to the gravity vector resulting in drift in both the x and y directions. A significant portion of this should be accounted for during the initialization process, so it was determined to use an alternate method instead.



Figure 4.16: Experiment Setup with LD-OEM 1000 Laser Scanner Mounted on Cart with Trimble S6 Surveying System in the Foreground

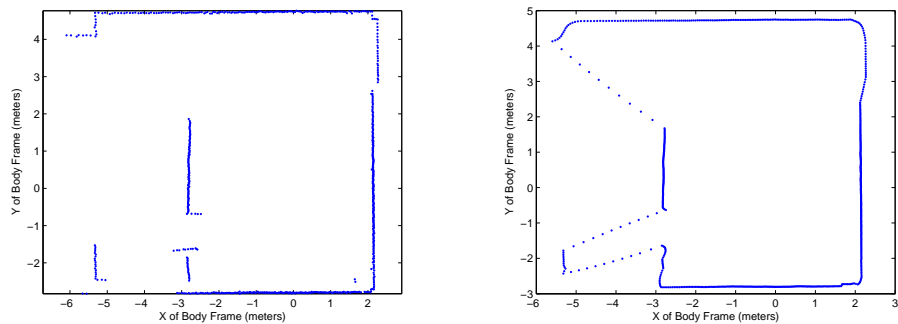
A Trimble S6 Total Station surveying system, also shown in Figure 4.16, was selected as an alternative method for comparison to provide accurate measurements within $4 \text{ mm} + 2 \text{ parts per million}$ [40]. While these measurements are suitable for a pseudo-truth source, timing is more of an issue with this system. Measurements are taken every second with the precision of only one second. This was determined not to be a limiting factor as the estimated path extracted from laser scanner data was most important. To align the Trimble and processed laser scan data a stationary vehicle for a period of time, followed by movement, would allow aligning the data sources. Because this system uses line of sight laser measurements it is not possible to test every trajectory as modeled in the simulation. The ANT center has a location to view most of the room, however it was not possible to go into the hallway and around the corner as detailed in Section 4.1.1. A 180 degree view of the ANT Center taken from the approximate position of the Trimble system is shown in Figure 4.2.4.

4.2.5 ANT Center Data Collection and Results. The simulation of the ANT Center provided an estimate of performance in navigation of the room by the laser



Figure 4.17: Panorama of the ANT Center Showing 180 Field of View

scanner using the histogram correlation method. While the simulation only modeled eight flat and perpendicular walls there are actually numerous noisy areas of the room, such as shelves placed along a wall, pipes running vertically near the corners, doors creating a different wall than the parallel adjacent wall, and also the temporary walls which were not straight, or parallel to existing walls. Also, the laser scanner moving on the cart had some vibration due to its height of placement so the cart could be easily moved without obstructing the view of the device. Filtering is meant to reduce some of these effects, however, degraded performance is to be expected. Side by side images of the same scan, both as measured, and then filtered at a setting of 15 are found in Figures 4.18(a) and 4.18(b). The scans are taken from the right half of the room with the door visible in the upper right corner and the entrance to the temporary walled office in the lower left. The filtering smooths the noisy walls along with small objects that were found, but also removes other features such as the entry way to the office, and it's interior wall.



(a) Laser Scan from the ANT Center as Measured (b) Laser Scan from the ANT Center Filtered

Figure 4.18: Identical Scan of the ANT Center, as measured and filtered at a setting of 15

Processing of the collected scans were processed at various filter settings and update rates. As previously seen, an update rate of 10 Hz, and a filter of 15 provided the most stable and accurate results. The ground track as measured by the Trimble survey station, along with the estimated trajectory by the histogram correlation algorithm are shown in Figure 4.19. The resulting x and y errors are plotted over time in Figure 4.20. The periodic nature of these errors is explained in Section 4.3. Due to the restriction of the Trimble system heading information is unavailable. Analysis of the measured laser scans show heading variations up to 15 degrees, and observation of the estimated heading is in agreement of the algorithm tracking the heading angle acceptably.

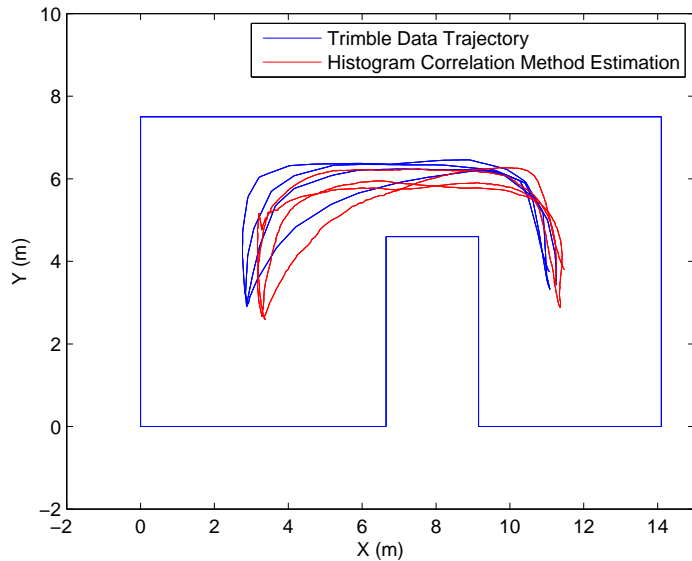


Figure 4.19: Comparison of Trimble Observed and Histogram Correlation Estimated Trajectory

Noticing the x direction has an error growth occurring at approximately 12 seconds with constant error after that led to further analysis of this point. Figure 4.21 shows the interpolated Trimble data points and the estimates as provided by the histogram correlation method. This confirms that at this time the estimated solution drifted away from the measurement, but then remained at this approximate error. This occurs as the laser scan is approximately the point (3.5,5), the point at which

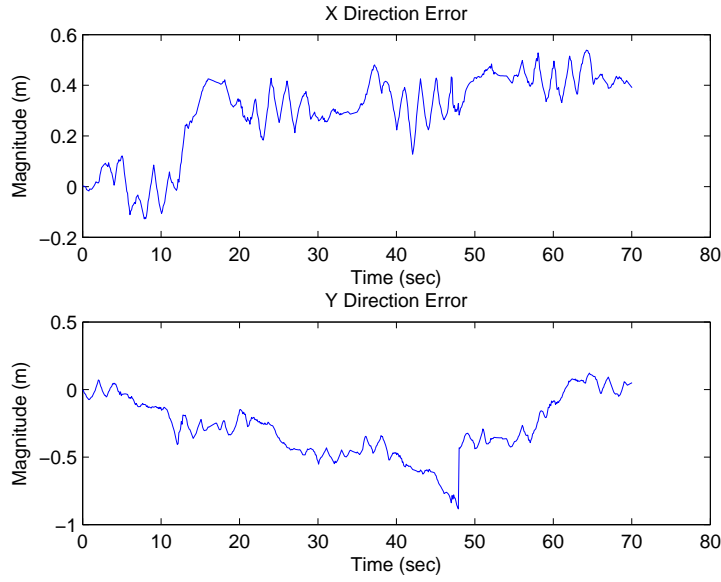


Figure 4.20: Error Growth in Each Direction

the temporary wall in the x direction becomes no longer visible. This was a point of concern for use of the algorithm in the ANT Center. While this single crossing was noted to be a problem, there were multiple other occurrences where this was not an issue as the vehicle passed near this same point, and another near (12,5) where the same effect would occur in this direction.

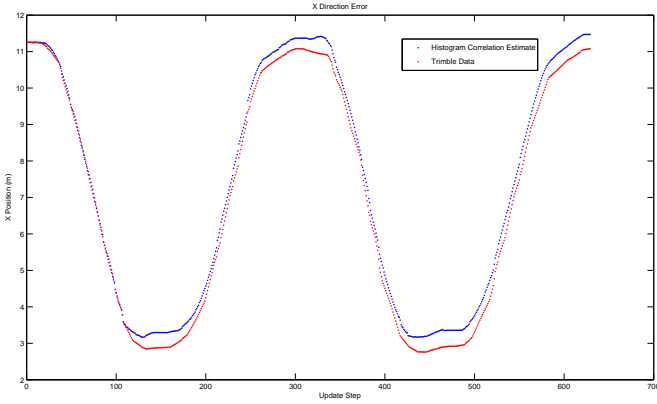


Figure 4.21: Estimated and Reference in X Direction Over Time

Performance in the y direction, as shown in Figure 4.22, shows similar behavior of error growth which happens more often than the x direction. These occur when the

scanner passes the temporary walls which lie in the y direction. Due to the geometry of the ANT Center the laser scanner this happens twice as often as the x direction, and performance is degraded because of this.

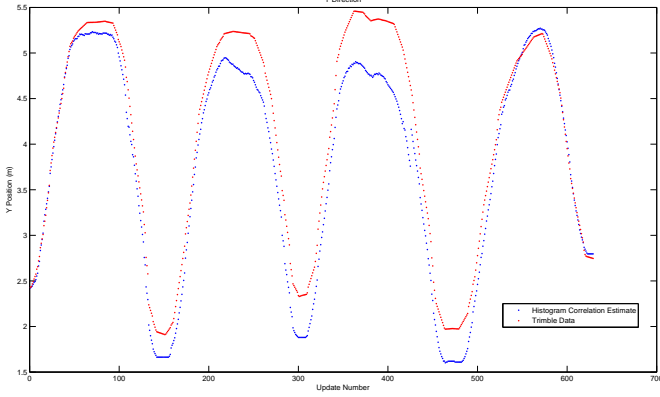


Figure 4.22: Estimated and Reference in Y Direction Over Time

4.2.6 Hallway Data Collection and Results. One important environment of interest in navigation of the vehicle discussed in this work is through hallway or corridor navigation. Concern has been discussed in previous applications when using the correlation method in a long hallway due to issues of limited visibility of the system. A laser scanner is able to measure numerous points in the walls parallel to it's movement while traversing the hallway positioning the vehicle between these walls well, but it is unable to measure the wall perpendicular providing the movement information of movement down the hallway. The LD-OEM 1000 shows improved results due to zits 360 degree field of view allowing measurement of an additional wall behind the vehicle, and also its higher resolution than other scanners often used for this method resulting in additional points found along the far walls.

While these benefits are expected to improve performance, navigation in the hallway still suffers from a near/far problem. When the scanner is operated less than a meter from 2 walls but at least an order of magnitude more from the others the histogram method correlations for translation will not perform equally well. When filtered properly the heading angle determination should perform well due to the

majority of laser measurements to be parallel lines that are easily correlated. An example of this with an excellent correlation spike is found in Figure 4.23. However, during calculation of the X and Y directions only one has a good correlation to work from as seen in Figure 4.24 and 4.25. Note: the X and Y shown here do not correspond to the navigation frame, but only to the correlation of these scans as they are rotated about the main direction angle found as detailed in Section 3.3.

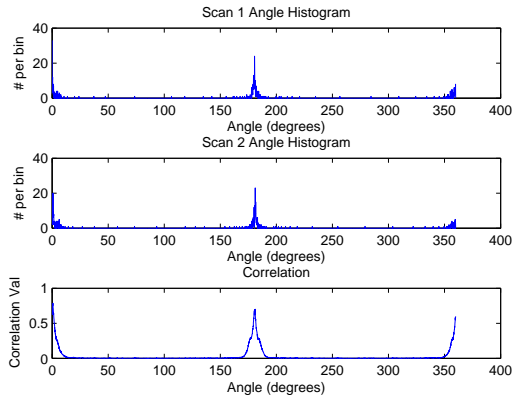


Figure 4.23: Example of Angle Correlation while Traveling Down a Hallway

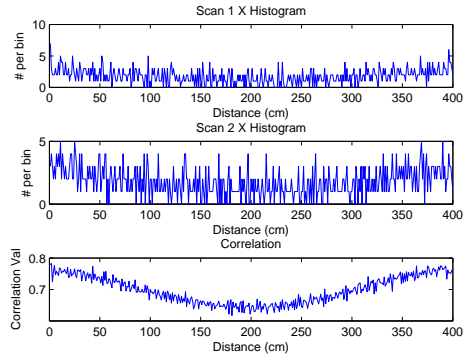


Figure 4.24: Example of the Bad Direction for Translation Correlation as a Result of Traveling Down a Hallway

Initial testing in the hallway environment was performed by walking the cart around all four hallways adjacent to the ANT Center. These hallways have a few peculiar aspects which provide additional visibility in directions perpendicular to the hallway direction, for example notches for drinking fountains, or office entryways.

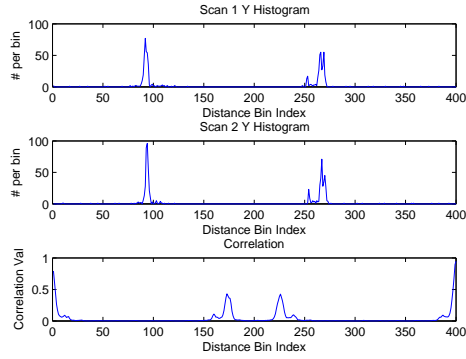


Figure 4.25: Example of the Good Direction for Translation Correlation as a Result of Traveling Down a Hallway

A sample data collect processed at four different angle filter settings is found in Figure 4.26. As expected the filter settings of 10 and 15 perform the best. Analysis of

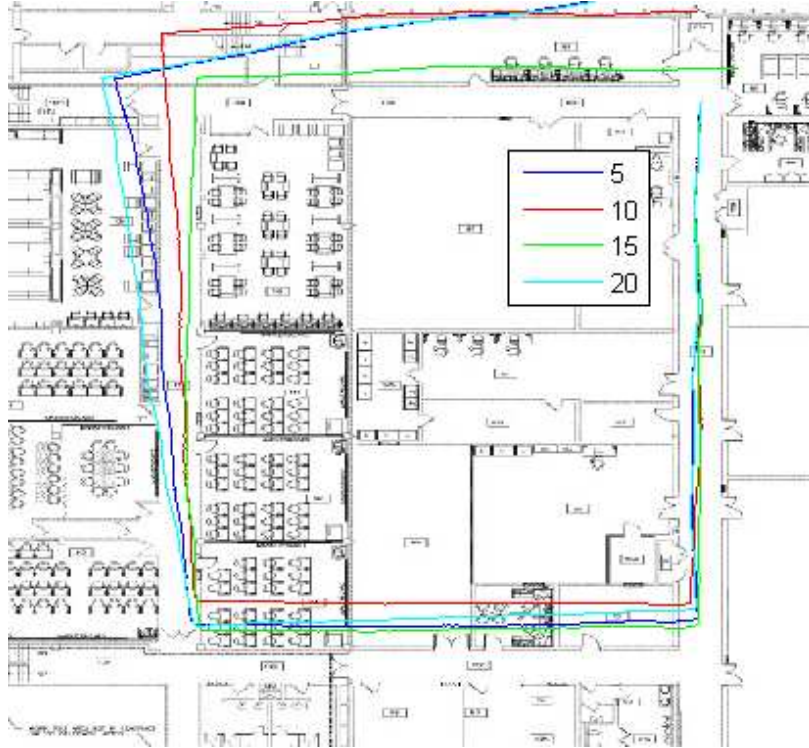


Figure 4.26: Estimated Path around Hallway using Different Filter Settings

these results produced a few interesting anomalies. At one portion of the first hallway traveled the scans estimated a backwards movement when a fairly consistent forward motion was used for the duration of the hallway. This coincides with a portion of the

hallway where there was minimal information in the other direction. For most of the movement throughout the hallways there were open doors allowing visibility of walls perpendicular to the hallway which aided in determining the lengthwise direction. The estimated backwards motion is shown in Figure 4.27(a) and is present in all filter settings as only the angle correlation calculation uses filtered data scans. The x and y translation calculations should be identical, but applied differently based upon the current estimated heading angle. This erroneous correlation occurs when there is minimal information in the one direction as shown by one corresponding scan taken in the area in Figure 4.27(b). This flawed translation calculation was noticed across many trials on collected on different days all occurring in the same location.

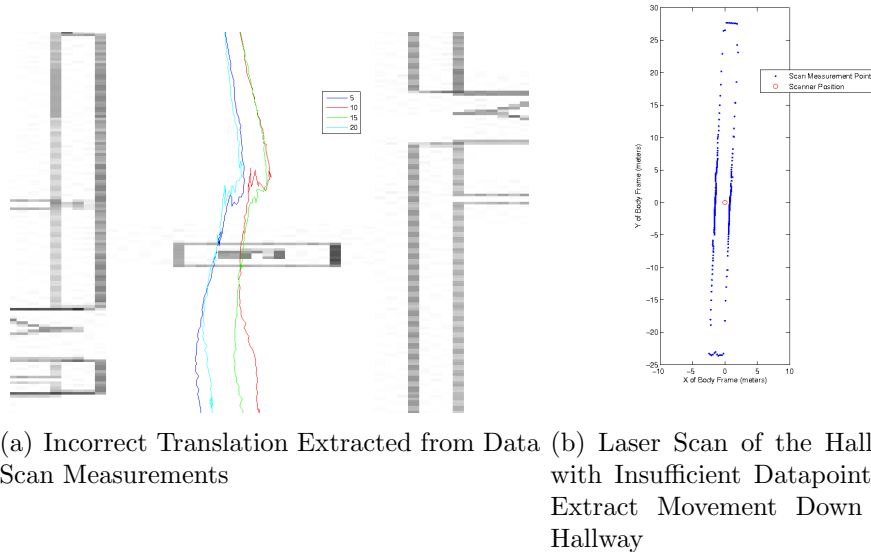


Figure 4.27: Poor Performance of the Algorithm While Traveling Down a Hallway

4.3 Comparison of Simulated and Experimental Data

To compare experimental data to the simulation data a similar trajectory was traveled using the cart, as compared in Figure 4.28. The simulated profile travels a similar trajectory in 80 seconds, while the experimental data travels across the room four times in 63 seconds.

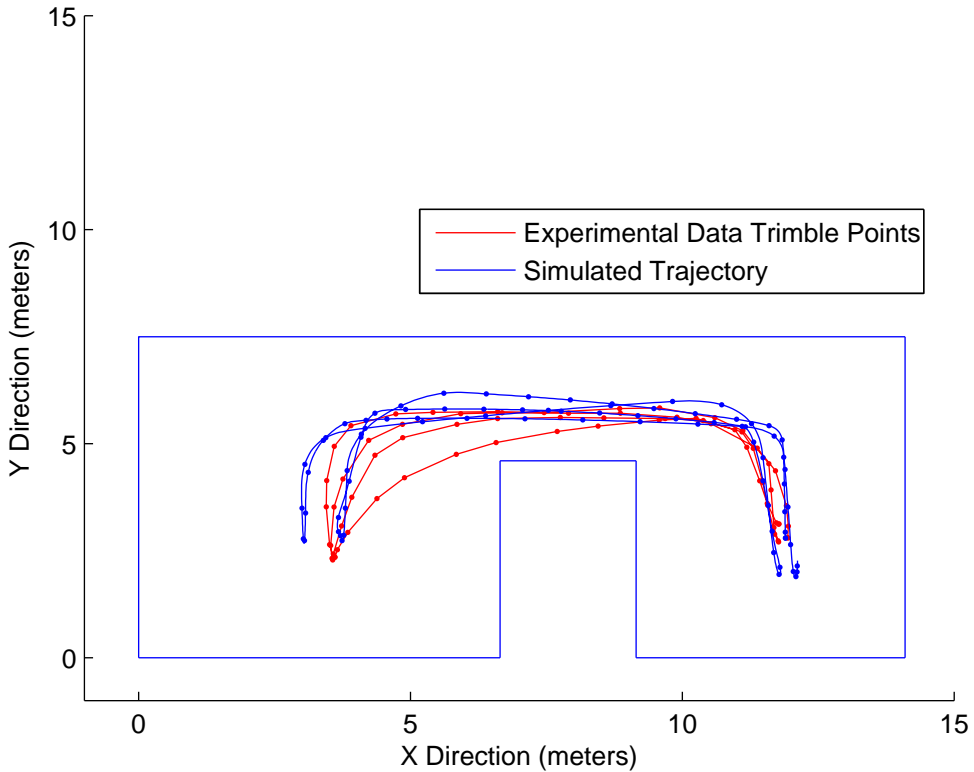


Figure 4.28: Simulated and Experimental Trajectory as Traveled in the ANT Center

The periodic nature of the error growth of the experimental data is due to the limitations in the Trimble measurement system. To analyze error growth over time the accurate one second timestamps were assumed to happen at exactly a 1 Hz rate, and points were linearly interpolated between the two points according to the time stamp of the rangefinder's data scan. This effect creates a jagged flight profile estimation where the curves become straightened. The periodic growth and decay of this is detailed in Figure 4.31 where the vehicle's path first travels away from the estimated path for a half second, and then back toward the estimated path for the next half second.

While Section 3.2.3 suggested that the simulation noise level of 2 cm was similar to actual performance of the laser scanner the results more similarly matched the noise

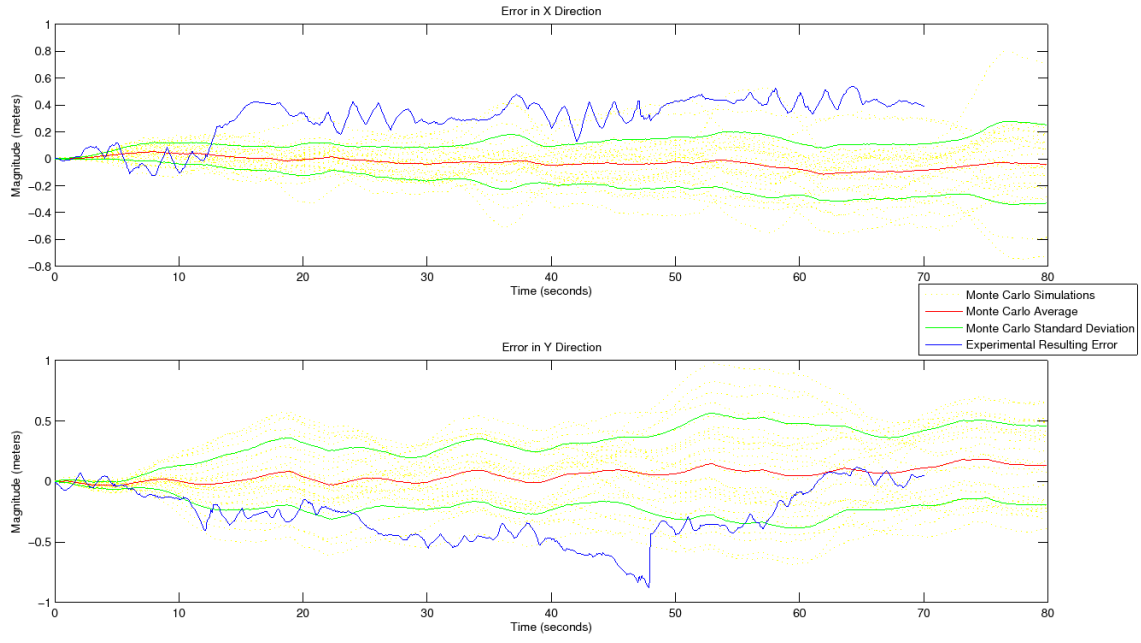


Figure 4.29: Comparison using 2 cm noise estimate

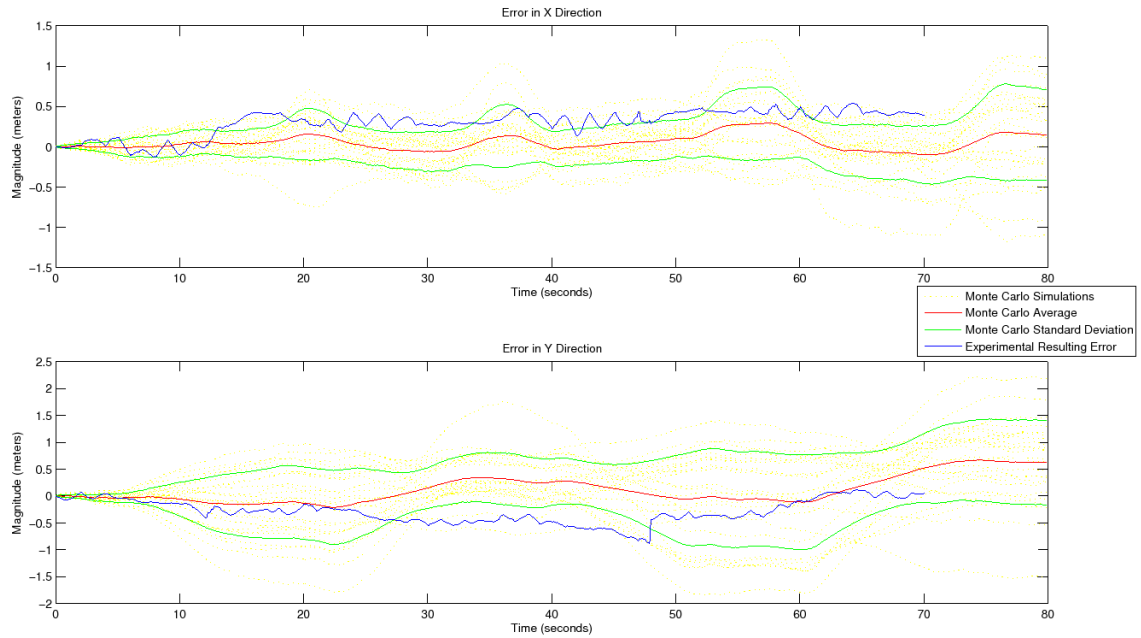


Figure 4.30: Comparison using 4 cm noise estimate

level expected by the LD-1000 data sheet of 4 cm. Each representative plot is shown in Figures 4.29 and Figures 4.30.

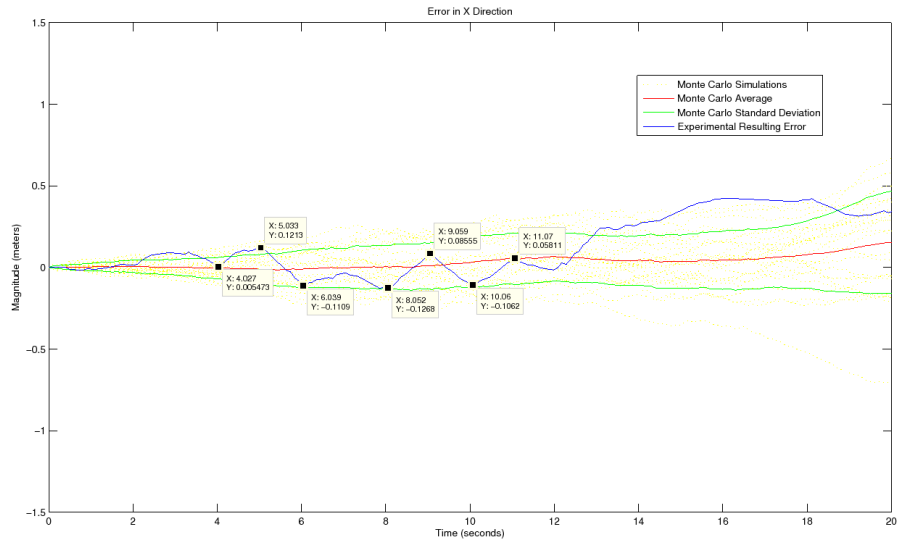


Figure 4.31: Periodic Line Fit Error Caused by Interpolation of Trimble Data

There were many factors contributing to degraded performance in the experimental setup that were not modeled in the simulation. These include the vibration in the scanner when mounted high on the cart, temporary walls which aren't perpendicular or parallel, additional pipes and shelves in the environment degrading scan performance, and the introduction of heading changes while the cart was moving.

V. Conclusions and Recommendations

This chapter overviews the achieved performance of the developed navigation solution using the histogram correlation algorithm method. Suggested improvements and relevant future testing experiments are also discussed.

5.1 Conclusion of Performance

5.1.1 Simulation. The MATLAB simulation developed for this work takes advantage of a realistic quadrotor simulator to provide realistic flight and therefore accurate performance expectations for any environment. It is easily modified to assist in analysis of the effects of update rate, sensor noise, and flight trajectory. Investigation into other variables such as the use of a different laser scanner are also possible. This framework is able to predict performance in a specific situation. With a high-fidelity environment model and predicted flight plan tuning parameters such as the size of the moving average filter can be adjusted for the optimal unaided navigation solution.

In simulation an update rate of 10 Hz was stable for all flight profiles tested, but performed worse than an update rate of 5 Hz or 1 Hz for most instances of the simulation. Often, the 1 Hz trials acquired errors that would not be acceptable for providing a navigation position solution. Rates slower than this are possible when operating in a limited environment, but they were not experimented with in this work. If the accuracy of the solution when using a 10 Hz update rate was prohibitive a simulation may assist in selecting the appropriate update rate for a given flight trajectory and environment.

5.1.2 Real World. The algorithms adapted for use in this thesis were only tested in a two dimensional environment due to the test setup available. Performance in this setting was evaluated in two distinct environments of interest, inside a moderately sized room, and in long hallways. Using appropriate tuning parameters for each

case yielded a valuable navigation solution in both cases. These specific values would need to be determined either through simulation or experimentation for each case.

Overall the most stable results with experimental data occurred when processing at an update rate of 10 Hz with a filter setting of 15. To improve performance these may be tweaked depending on the environment. For better results the update rate can be lowered, yet this may cause the solution to become unstable. With additional processing and system modeling this may be avoidable, or at least acknowledged by the algorithm in real time.

In conclusion, the histogram correlation algorithm applied in this work was shown to successfully navigate a realistic environment where a quadrotor may be utilized. The current calculated position and heading solution provided by the algorithm is acceptable for vehicles using short flight times of less than 5 min in open areas. Application of the algorithm in hallway navigation shows great promise providing a stable heading determination along with tracking movement perpendicular to the hallway. However, additional modifications may be necessary to assist in the translation parallel to the hallway. The results shown in this thesis show promising potential in the use of using a LADAR to provide a position and heading solution over longer flights. This may be accomplished with additional processing or by coupling laser measurements with an additional sensor.

5.2 Suggested Improvements to the Current Algorithm

5.2.1 Additional Filtering of Laser Scan Data. Filtering laser scan measurements when performing the rotation angle calculations proved to be beneficial, even necessary, to provide a stable solution. A similar filtering method may improve translation correlations. The histogram correlation method tends to suffer from a near far problem where many points are generated when a scanner is in closer proximity to a single wall than any others. The number of points found on this wall may greatly outnumber the points measured in the rest of the environment. This effect is most apparent in a hallway environment. Additional filtering methods may include deter-

mining the proximity of consecutive laser scan measurements to generate a balanced number of data points along each wall, and each direction.

5.2.2 Integration with Additional Hardware or Software. As with most sensors used in navigation they are often combined to provide a better overall estimate using a type of Kalman Filter. Combining the laser scanner detailed in this thesis with a MEMs IMU would provide significant improvement as each sensor behaves differently. The IMU has a fast update rate where the laser scanner is slower and would be capable of limiting a portion of the drift in the IMU. One instance of this would be when traveling in the hallway environment and the independent laser scanner solution estimated reverse movement, as discussed in Section 4.2.6. This could be avoided because the system model used in the Kalman filter would understand this movement to be impossible by the vehicle, especially with input from an IMU, and put little weight into factoring in the measurement update. Additional aiding techniques may be applied using a Kalman filter without additional sensors and rely on the system model to weigh updates appropriately.

An alternative method of using an IMU to aid the developed method would be to correct the scans according to the vehicle's attitude so that a significant portion of the skewing behavior would be mitigated. This would not be as effective for this application using the quadrotor where attitude angles of less than eight degrees are expected during operation in relatively small environments. If a vehicle with more extreme flight dynamics, or operation in a larger environment such as outdoor in a city street, the performance may be increased when performing these corrections.

5.2.3 Testing in a 3D Environment. Ultimately this work was developed to operate on a quadrotor platform and would greatly benefit from flight testing. Performing such tests in the ANT Center where a Vicon motion capture system can provide real time true position and vehicle attitude would be ideal. This was not pursued because the quadrotor in development to fly the LADAR unit is not currently flying. Other experimentation using the motion tracking was not performed because

of the limited translation available to stay within the system's field of view. Under this setup truth data is available at a much higher rate than the Trimble surveying system which is also limited to positioning information.

Using the immediate attitude information available by this system could provide a more accurate framework for the investigation into direct aiding of the laser scan data correcting for pitch and roll angles. This would assist in quantifying the benefit of coupling an IMU or other device during flight.

5.2.4 Future Topics of Interest. Due to limited experimental data and simulations which were too similar, the error growth necessary when implementing a Kalman filter, was not clearly identified. The error growth was shown to be strongly influenced by the environment and also by the flight trajectory. This was witnessed in the long simulation detailed in the end of chapter 4. A better characterization of the error growth is recommended.

Bibliography

1. AG, SICK. *LD-OEM 1000 to 5100 Laser Measurement System Operating Instructions*, 2009.
2. AG, SICK. *LD-OEM 1000 Online Datasheet*, 2011. URL <https://www.mysick.com/partnerPortal/ProductCatalog/DataSheet.aspx?ProductID=33784#>.
3. Arras, Kai O. *CAS Robot Navigation Toolbox*. Center for Autonomous Systems, March 2004.
4. Bachrach, Abraham Galton. *Autonomous Flight in Unstructured and Unknown Indoor Environments*. Master's thesis, Massachusetts Institute of Technology, September 2009.
5. Bates, Dustin P. *Navigation Using Optical Tracking of Objects at Unknown Locations*. Master's thesis, Ohio University, 2007 March.
6. Bedkowski, Janusz, Maciej Kretkiewicz, and Andrezej Masłowski. *3D laser range finder simulation based on rotated LMS SICK 200*. Technical report, Research Institution of Automation and Control, Intelligent Mobile Systems Division, Aleje Jerozolimskie 202, Warsaw, Poland, 2008.
7. Borenstein, J., H.R. Everett, L. Feng, Contributing Authors S.W. Lee, and R.H. Byrne. *"Where am I?" Sensors and Methods for Mobile Robot Positioning*. Technical report, University of Michigan, April 1996.
8. Bosse, M. and J. Roberts. "Histogram Matching and Global Initialization for Laser-only SLAM in Large Unstructured Environments". *Robotics and Automation, 2007 IEEE International Conference on*, 4820 –4826. 10-14 2007. ISSN 1050-4729.
9. Concepts, Advanced Scientific. *Advanced Scientific Concepts Inc Product Specifications*. ASC, Inc., 2010. URL <http://www.advancedscientificconcepts.com/products/tigereye.html>.
10. D Michael Sobers, Jr, Girish Chowdhary, and Eric N Johnson. "Indoor Navigation for Unmanned Aerial Vehicles". *AIAA Guidance, Navigation, and Control Conference*, 1:29, August 2009.
11. Derenick, Jason and Thomas Miller. *Sick LIDAR Matlab/C++ Toolbox*. Vision, Assistive Devices, and Experimental Robotics Laboratory, 2008. URL <http://www.cas.kth.se/toolbox>.
12. Deyle, Travis. *MIT's DARPA Urban Grand Challenge*. Massachusetts Institute of Technology, 2008.

13. Duda, Richard O. and Peter E. Hart. “Use of the Hough Transformation to Detect Lines and Curves in Pictures”. *Communications of the ACM*, 15:11–15, January 1972.
14. Feng Lu, Evangelos Milios. “Robot Pose Estimation in Unknown Environments by Matching 2D Range Scans”. *IEEE Computer Society Conference on Computer Vision and Pattern Recognition*, 1:935–938, June 1994.
15. Geosystems, Leica. *Leica Geosystems HDS6100 Brochure*, 2009. URL <http://www.leica-geosystems.com/hds>.
16. Gillis, Brian and Jeffrey Kozak. *RIT Micro Air Vehicles*. Technical report, Rochester Institute of Technology, 2005. URL <http://edge.rit.edu/content/0ldEDGE/public/Archives/P05001/Files/PDR.pdf>.
17. de Haag Zhen Zhu Andrey Soloviev Frank van Graas, Maarten Uijt. *Tightly-Integrated LADAR/INS Algorithm Development to Support Urban Operations*. Technical report, Ohio University, Avionics Engineering Center, Russ College of Engineering and Technology School of Electrical Engineering and Computer Science Avionics Engineering Center Athens, OH 45701, February 2009.
18. Gutmann, J.-S., Thilo Weigel, and B. Nebel. “Fast, accurate, and robust self-localization in polygonal environments”. *Intelligent Robots and Systems, 1999. IROS '99. Proceedings. 1999 IEEE/RSJ International Conference on*, volume 3, 1412 –1419 vol.3. 1999.
19. Uijt de Haag, M., D. Venable, and A. Soloviev. “Implementation of a Flash-LADAR aided inertial navigator”. *Position, Location and Navigation Symposium, IEEE/ION*, 1:560 –567, May 2008.
20. Hamilton, Nicolas. *Non Linear Quadrotor Simulator*. Advanced Navigation Technology Center, 2010.
21. J. Borenstein, L. Feng, H.R. Everett and D. Wehe. “Mobile Robot Positioning - Sensors and Techniques”. *Journal of Robotic Systems, Special Issue on Mobile Robots*, 14:231–249, April 1997.
22. Kim, Myoung-Ho, Min Kim, and Kuae-Hi Lee. “Localization Method Using Vector-Histogram”. *Smart Manufacturing Application, 2008. ICSMA 2008. International Conference on*, 581 –584. 9-11 2008.
23. Legland, David. *geom3d Matlab Toolbox*. Matlab File Exchange, 2010. URL <http://www.mathworks.com/matlabcentral/fileexchange/224484-geom3d>.
24. LiDAR, Velodyne. *Velodyne LiDAR Website*, 2010. URL <http://www.velodyne.com/lidar/lidar.aspx>.
25. Lindsey, Kevin. “Kevin Lindsey Software Development”. URL <http://www.kevlinddev.com/geometry/index.htm>. Scalable Vector Graphics and JavaScript Geometry Toolbox.

26. Lingemann, K., H. Surmann, A. Nuchter, and J. Hertzberg. “Indoor and outdoor localization for fast mobile robots”. *Intelligent Robots and Systems, 2004. (IROS 2004). Proceedings. 2004 IEEE/RSJ International Conference on*, volume 3, 2185 – 2190 vol.3. 28 2004.
27. MaxBotix. *LV-MaxSonar-EZ0 Data Sheet*, 2011. URL <http://www.maxbotix.com/uploads/LV-MaxSonar-EZ-Datasheet.pdf>.
28. Maybeck, Peter S. *Stochastic Models, Estimation, and Control*, volume 1. Navtech Book and Software Store, 1994.
29. Misra, Pratap and Per Enge. *Global Positioning System, Signals, Measurement, and Performance*. Ganga-Jamuna Press, 2nd edition, 2006.
30. Ng, Teck Chew, Javier Ibaez Guzmn, and Jin Chang Tan. “Development of a 3D LADAR System for Autonomous Navigation”. *IEEE Conference on Robotics, Automation and Mechatronics*, volume 2, 792–797. December 1-3 2004.
31. Nguyen, Viet, Agostino Martinelli, Nicola Tomatis, and Roland Siegwart. “A Comparison of Line Extraction Algorithms using 2D Laser Rangefinder for Indoor Mobile Robotics”. *IEEE/RSJ International Conference on Intelligent Robots and Systems*, 1:1929–1934, Aug 2005.
32. Olson, E.B. “Real-time Correlative Scan Matching”. *2009 IEEE International Conference on Robotics and Automation*, 4387 –4393. may. 2009. ISSN 1050-4729.
33. Qiu, Quan and Jianda Han. “Laser scan matching using multiplex histograms with feature components”. *IEEE International Conference on Robotics and Biomimetics (ROBIO)*, 275 –280. 19-23 2009.
34. Röfer, Thomas. “Using Histogram correlation to Create Consistent Laser Scan Maps”. *Proceedings of the IEEE International Conference on Robotics Systems*, 1:625–630, December 2002.
35. Soloviev, A. de Haag. “Three-Dimensional Navigation with Scanning Ladars: Concept & Initial Verification”. *IEEE Transactions on Aerospace and Electronic Systems*, 46:14–31, Jan 2010.
36. Soloviev, Andrey. “Tight Coupling of GPS, Laser Scanner, and Inertial Measurements for Navigation in Urban Environments”. *Position, Location and Navigation Symposium, IEEE/ION*, 1:511–525, May 2008.
37. Stone, Peter, Patrick Beeson, Tekin Mericli, and Ryan Madigan. *DARPA Urban Challenge Technical Report*. Technical report, Austin Robot Technology, 2007. URL http://personal.traclabs.com/_pbeeson/papers/Stone-tr-07.pdf.
38. Theodosios Pavlidis, Steven L. Horowitz. “Segmentation of Plane Curves”. *IEEE Transactions on Computers*, C-23:860 – 870, August 1974.
39. Titterton, David H. and John L. Weston. *Strapdown Inertial Navigation Technology*. The Institution of Electrical Engineers and The American Institute of Aeronautics and Astronautics, 2 edition, 2004.

40. Trimble. *Trimble S6 Total Station Datasheet*, 2009. URL http://www.trimble.com/trimbleS6_ds.asp.
41. Vandorpe, J., H. Van Brussel, and H. Xu. “Exact Dynamic Map Building for a Mobile Robot using Geometrical Primitives Produced by a 2D Range Finder”. *Proceedings of the 1996 IEEE International Conference on Robotics and Automation*, 1:901–908, 1996.
42. Weiss, G., C. Wetzler, and E. von Puttkamer. “Keeping track of position and orientation of moving indoor systems by correlation of range-finder scans”. *Intelligent Robots and Systems*, 1:595 – 601, 1994.
43. Zehong, Xu, Liu Jilin, and Xiang Zhiyu. “Scan matching based on CLS relationships”. *Robotics, Intelligent Systems and Signal Processing, 2003. Proceedings. 2003 IEEE International Conference on*, volume 1, 99 – 104 vol.1. 8-13 2003.

REPORT DOCUMENTATION PAGE

*Form Approved
OMB No. 0704-0188*

The public reporting burden for this collection of information is estimated to average 1 hour per response, including the time for reviewing instructions, searching existing data sources, gathering and maintaining the data needed, and completing and reviewing the collection of information. Send comments regarding this burden estimate or any other aspect of this collection of information, including suggestions for reducing this burden to Department of Defense, Washington Headquarters Services, Directorate for Information Operations and Reports (0704-0188), 1215 Jefferson Davis Highway, Suite 1204, Arlington, VA 22202-4302. Respondents should be aware that notwithstanding any other provision of law, no person shall be subject to any penalty for failing to comply with a collection of information if it does not display a currently valid OMB control number. PLEASE DO NOT RETURN YOUR FORM TO THE ABOVE ADDRESS.

1. REPORT DATE (DD-MM-YYYY)	2. REPORT TYPE	3. DATES COVERED (From — To)		
24-03-2011	Master's Thesis	Sept 2009 — Mar 2011		
4. TITLE AND SUBTITLE Two Dimensional Positioning and Heading Solution for Flying Vehicles using a Line-Scanning Laser Radar (LADAR)		5a. CONTRACT NUMBER 5b. GRANT NUMBER 5c. PROGRAM ELEMENT NUMBER		
6. AUTHOR(S) Brady Christel		5d. PROJECT NUMBER 5e. TASK NUMBER 5f. WORK UNIT NUMBER		
7. PERFORMING ORGANIZATION NAME(S) AND ADDRESS(ES) Air Force Institute of Technology Graduate School of Engineering and Management (AFIT/EN) 2950 Hobson Way WPAFB OH 45433-7765		8. PERFORMING ORGANIZATION REPORT NUMBER AFIT/GE/ENG/11-04		
9. SPONSORING / MONITORING AGENCY NAME(S) AND ADDRESS(ES) INTENTIONALLY LEFT BLANK		10. SPONSOR/MONITOR'S ACRONYM(S) 11. SPONSOR/MONITOR'S REPORT NUMBER(S)		
12. DISTRIBUTION / AVAILABILITY STATEMENT APPROVAL FOR PUBLIC RELEASE; DISTRIBUTION IS UNLIMITED. This material is declared a work of the U.S. Government and is not subject to copyright protection in the United States.				
13. SUPPLEMENTARY NOTES				
14. ABSTRACT Emerging technology in small autonomous flying vehicles requires the systems to have a precise navigation solution in order to perform tasks. In many critical environments, such as indoors, GPS is unavailable necessitating the development of supplemental aiding sensors to determine precise position. This research investigates the use of a line scanning laser radar (LADAR) as a standalone two dimensional position and heading navigation solution and sets up the device for augmentation into existing navigation systems. A fast histogram correlation method is developed to operate in real-time on board the vehicle providing position and heading updates at a rate of 10 Hz. LADAR navigation methods are adapted to 3 dimensions with a simulation built to analyze performance loss due attitude changes during flight. These simulations are then compared to experimental results collected using SICK LD-OEM 1000 mounted a cart traversing. The histogram correlation algorithm applied in this work was shown to successfully navigate a realistic environment where a quadrotor in short flights of less than 5 min in larger rooms. Application in hallways show great promise providing a stable heading along with tracking movement perpendicular to the hallway.				
15. SUBJECT TERMS line scanning laser radar, micro air vehicle, navigation				
16. SECURITY CLASSIFICATION OF: a. REPORT b. ABSTRACT c. THIS PAGE U U U		17. LIMITATION OF ABSTRACT UU	18. NUMBER OF PAGES 86	19a. NAME OF RESPONSIBLE PERSON Michael J. Stepaniak, Lt Col, USAF (ENG) 19b. TELEPHONE NUMBER (include area code) (937)785-3636ext4603;Michael.Stepaniak@afit.edu